Physics – Uspekhi **52** (7) 659 – 685 (2009) © 2009 Uspekhi Fizicheskikh Nauk, Russian Academy of Sciences

REVIEWS OF TOPICAL PROBLEMS PACS numbers: 12.38.Mh, **25.75.–q**, 52.27.Ny, **61.85.+p**

Energy losses in relativistic plasmas: QCD versus QED

S Peigné, A V Smilga

DOI: 10.3367/UFNe.0179.200907a.0697

Contents

Abstract. We review the problem of evaluating the energy loss of an ultrarelativistic charged particle crossing a thermally equilibrated high-temperature e^+e^- or quark–gluon plasma. The average energy loss ΔE depends on the particle energy E and mass M, the plasma temperature T, the QED (QCD) coupling constant α (α_s), and the distance L the particle travels in the medium. Two main mechanisms contribute to the energy loss: elastic collisions and bremsstrahlung. For each contribution, we use simple physical arguments to obtain the functional dependence $\Delta E(E, M, T, \alpha_{(s)}, L)$ in different regions of the parameters. The suppression of bremsstrahlung due to the Landau–Pomeranchuk–Migdal effect is relevant in some regions. In addition, radiation by heavy particles is often suppressed for kinematic reasons. Still, when the travel distance L is not too small, and for large enough energies [$E \gg M^2/(\alpha T)$ in the Abelian case and $E \gg M/\sqrt{\alpha_s}$ in the non-Abelian case], radiative losses dominate over collisional ones. We rederive the known results and make some new observations. In particular, we emphasize that for light particles ($m^2 \ll \alpha T^2$), the difference in the behavior of $\Delta E(E, m, T, \alpha_{(s)}, L)$ in QED and QCD is mostly due to the different problem setting in these two cases. In QED, it is natural to study the energy losses of an electron coming from infinity. In QCD, the quantity of physical interest is the medium-induced energy loss of a parton produced *within* the medium. In the case of an electron produced within a QED plasma, the medium-induced radiative energy loss $\Delta E_{\rm rad}$ behaves similarly to $\Delta E_{\rm rad}$ in QCD (in particular, $\Delta E_{\rm rad} \propto L^2$ at small L), despite the photon and gluon radiation spectra being drastically different because the bremsstrahlung cones for soft gluons are broader than for soft photons. We also show that the average radiative loss of an 'asymptotic light parton' crossing a QCD plasma is similar to that of an asymptotic electron crossing a QED plasma. For heavy particles ($M^2 \gg \alpha T^2$), the difference between $\Delta E_{\rm rad}$ in QED and in QCD is more pronounced, even when the same physical situation is considered.

1. Introduction

Evaluating the energy loss of a charged particle passing through usual matter is a standard problem in nuclear physics, studied very well both theoretically and experimentally (see, e.g., Ref. [1]). It is known, for example, that for heavy particles (protons) of not too high an energy, the main contribution to the energy loss is made by collisions with individual atomic electrons, while for light particles (electrons) of similar energies, it is made by bremsstrahlung.

The energy loss problem can also be posed for a particle passing through a hot ultrarelativistic plasma.[1] In particular, one may ask what happens if a particle carrying a *color* charge passes through a hot QCD medium. In the limit where the medium temperature T is very high, $T \gg \Lambda_{\rm QCD}$, this medium is a quark–gluon plasma (QGP), i.e., a system of quarks and gluons with a small effective Coulomb-like interaction $\alpha_s(T) \ll 1$.[2] Of course, colored particles do not exist as asymptotic states, but we can imagine several thought experiments where the energy lost by an energetic parton

S Peigné, A V Smilga SUBATECH, UMR 6457, Université de Nantes
Ecole des Mines de Nantes, IN2P3/CNRS,
4 rue Alfred Kastler, 44307 Nantes cedex 3, France
E-mail: peigne@subatech.in2p3.fr, smilga@subatech.in2p3.fr

Received 26 November 2008, revised 10 March 2009
Uspekhi Fizicheskikh Nauk **179** (7) 697 – 726 (2009)
DOI: 10.3367/UFNr.0179.200907a.0697
Translated by S Peigné, A V Smilga; edited by A M Semikhatov

[1] In this paper, we consider thermally equilibrated and nonexpanding (static) plasmas.

[2] We use the term QGP in this restricted sense, which is a natural generalization of the conventional definition of a plasma [2]. When E Shuryak first proposed this name, he had this analogy in mind [3]. Unfortunately, in realistic heavy-ion collisions, the temperature reached

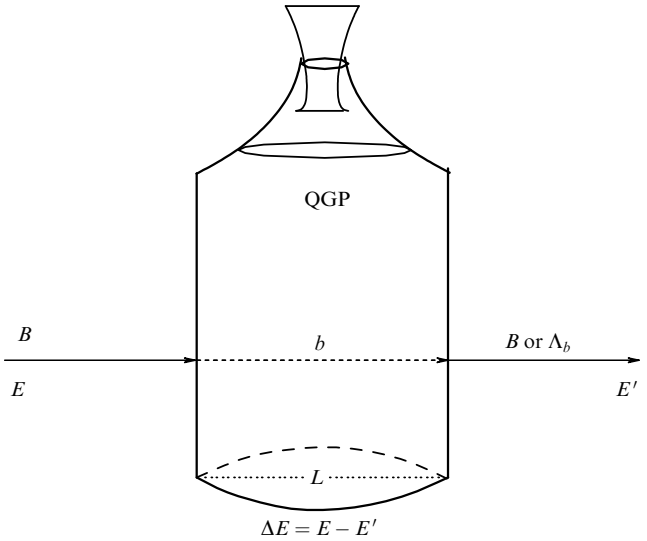

Figure 1. A heavy quark passes through a thermos bottle filled with the QGP.

crossing a QGP could in principle be measured. We consider a fast heavy meson (for example, a B-meson), consisting of a heavy quark and a light antiquark, coming from infinity (i.e., created in the remote past) and entering a tiny thermos bottle filled with the QGP on a laboratory table, as depicted in Fig. 1. In the hot environment, the heavy quark sheds its light partner and travels through the plasma losing its energy. When it leaves the bottle, it picks up a light antiquark or two light quarks to form a heavy colorless hadron. The difference in energy between the incoming meson and the outgoing heavy hadron roughly coincides with the heavy-quark energy loss.

This situation is probably the cleanest one from the theoretical standpoint. If the heavy quark mass is very large, $M \gg T$, the density of such quarks in the plasma is exponentially suppressed, and thus the passing heavy quark is tagged. But it is not possible, of course, to do such an experiment in reality. Hot QCD matter is produced in heavy-ion collisions for a few 10^{-23} of a second, and studying its interaction with a B-meson beam is impossible. It is possible, however, to access the energy loss of heavy or light particles produced *within* the plasma (via a hard partonic subprocess). A quark–antiquark pair created with a large relative transverse momentum in a hard partonic process gives rise to two distinct hadron jets. In heavy-ion collisions, the energy loss of the quark between its production and its escape from the QGP softens the p_T-spectrum of the leading hadrons in the associated jet, compared to the case of proton–proton collisions. This effect, called *jet quenching* and first anticipated by Bjorken [4], is now well established by the RHIC experiments [5–8].[3] A similar effect in cold nuclear matter at lower energies, namely, the attenuation of hadron energy distributions in deep inelastic scattering on nuclei, has been observed by the HERMES [10] and CLAS [11] collaborations.

is not high enough to have $\alpha_s(T) \ll 1$, and whether the system can be reliably described perturbatively is questionable. In this paper, we only consider a situation where the effective coupling is small and the perturbation theory applies.

[3] See Ref. [9] for a recent review on jet quenching.

Considering a parton produced in a (perturbative) QGP, there are two distinct cases. Either the produced parton is light or it is a heavy quark. For light partons of a sufficiently high energy $E \gg T$, the dominant energy loss mechanism (at not too small L) is gluon bremsstrahlung. This problem was previously considered in Refs [12–22]. To correctly evaluate radiative losses, it is important to take the generalization of the Landau–Pomeranchuk–Migdal (LPM) effect [23–25] in QCD into account. In brief, bremsstrahlung is a process where the radiation field accompanying a charged particle is shed. But a newborn 'undressed' particle must first 'dress' in its proper field coat before it can radiate again. If the time needed for such dressing (*formation time*) is large, the radiation intensity and hence the radiative energy loss are suppressed. For heavy quarks, bremsstrahlung is further suppressed compared to the light parton case [26] and the relative contribution of collisional losses increases. When the mass of the particle is not too large, $M \ll \sqrt{\alpha ET}$ in QED and $M \ll \sqrt{\alpha_s}\, E$ in QCD, and the travel distance L is not too small, radiative losses still dominate over collisional ones.

Our goal is to rederive and explain the results in a relatively simple way. We do not attempt to perform precise calculations (as regards radiative losses, they are very difficult, maybe impossible to do in a model-independent way) and only give the physical reasoning elucidating the parameter dependence of $\Delta E(E, M, T, \alpha_{(s)}, L)$ in different regions of the parameters. This physical emphasis and an accurate analysis of the radiation spectra for light and heavy particles are some distinguishing features of our review compared to review [27].

As emphasized above, studying the energy loss of a parton produced in a QGP is of phenomenological interest to heavy-ion collisions. It is, however, also instructive to discuss the problem of energy loss in QED. In this case, it is more natural to consider an asymptotic (on-shell) particle entering and then leaving a domain containing the ultrarelativistic e^+e^- plasma, but the production of a charged particle *within* the QED plasma can also be considered in principle.[4] Thus, we found it useful to calculate the energy loss of an ultrarelativistic charged particle in every different situation we can think of, even though some of them are academic.

In Section 2, we first discuss the collisional contribution to the energy loss, considering the cases of QED and QCD, and of heavy and light particles. For collisional losses, the way the particle is produced (in the remote past outside the plasma or inside the plasma) is not important. In Sections 3 and 4, we discuss the radiative energy loss of an asymptotic particle crossing a high-temperature plasma. Section 3 is devoted to QED, where this physical situation is more natural. In Section 4, we study the similar problem in QCD, where the 'asymptotic' partons should be understood as constituents of colorless hadrons when entering the plasma. In Section 5, we consider the case of a particle produced in a plasma, both in QED and QCD. We show there that the quadratic dependence of the induced radiative loss on the plasma size L at small enough L is not a feature specific to QCD. It also holds in QED with the same parametric dependence of the coefficient of L^2 (although logarithmic factors may differ). The differential gluon and

[4] For instance, we can think of the energy loss of a charged lepton produced in a heavy-ion collision (although it would be small in this case, due to the smallness of the QGP size compared to the lepton mean free path).

photon radiation spectra are qualitatively different, however. Because this might be useful to jet-quenching phenomenology, the induced gluon energy spectra corresponding to light and heavy quark radiation are discussed in some detail. Finally, we briefly summarize and give some general remarks in Section 6.

2. Collisional energy loss of a fast charged particle

The collisional loss of a fast charge crossing a hot plasma was first calculated by Bjorken [4]. This was done in the context of QCD, and was the basis of Bjorken's proposal to use jet quenching as a signature of QGP. Bjorken's result for the collisional loss (per unit distance) of an energetic light parton (light quark q or gluon g) is given by

$$\left.\frac{\mathrm{d}E_{\mathrm{coll}}}{\mathrm{d}x}\right|_{\mathrm{q,g}} = C_{\mathrm{R}}\pi\alpha_{\mathrm{s}}^2 T^2\left(1+\frac{n_{\mathrm{f}}}{6}\right)\ln\frac{ET}{\mu^2}, \tag{2.1}$$

where n_{f} is the number of thermally equilibrated quark flavors, $C_{\mathrm{R}} = C_{\mathrm{F}} = 4/3$ (quark) or $C_{\mathrm{R}} = N_{\mathrm{c}} = 3$ (gluon), and μ is an effective infrared cutoff. To the logarithmic accuracy, to which (2.1) is derived, μ can be taken as the Debye screening mass in the QGP, $\mu \sim gT$.

More detailed studies of the collisional losses in QED and QCD plasmas were performed, for instance, in Refs [28–34]. We review this issue below, emphasizing the difference between the two cases of a *tagged* (heavy) and *untagged* (light) particle.

2.1 Hot QED plasma

2.1.1 Ultrarelativistic muon. We consider the case of an ultrarelativistic muon of mass M and four-momentum $P = (E, \mathbf{p})$ passing through a hot $\mathrm{e}^+\mathrm{e}^-$ plasma of temperature T, with $E \gg M \gg T$. The last inequality ensures that there are no muons in the heat bath. The muon can lose its energy in either Coulomb collisions with electrons and positrons (Fig. 2a) or Compton collisions with photons (Fig. 2b).

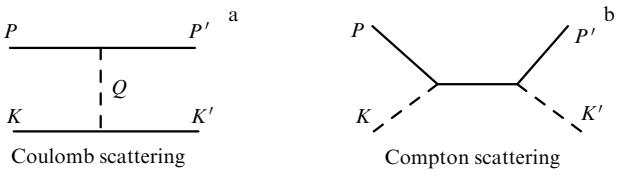

Figure 2. Typical graphs for collisions of a muon with plasma particles.

We first consider the losses due to Coulomb scattering. The differential Coulomb[5] cross section is given by

$$\frac{\mathrm{d}\sigma_{\mathrm{Coulomb}}}{\mathrm{d}t} \sim \frac{\alpha^2}{(t-\mu^2)^2}, \tag{2.2}$$

where $t \equiv Q^2 = (K-K')^2$ is the Mandelstam invariant momentum transfer and $\mu \sim eT$ is the Debye screening mass in the QED plasma. The total Coulomb scattering cross section is given by

$$\sigma_{\mathrm{Coulomb}} \sim \frac{\alpha^2}{\mu^2} \sim \frac{\alpha}{T^2}. \tag{2.3}$$

The momenta K and K' in Fig. 2 refer to thermal particles and are of the order of T. We note that they are slightly off the mass shell, $K^2 \sim K'^2 \sim \mu^2$, due to medium effects, which does not affect the estimates below, however. Since the integral for the total collisional loss is saturated in the region $|t| \gg \mu^2$ (as we see in a moment), we can write $t = -2KQ = -2(|\mathbf{K}|Q_0 - \mathbf{KQ})$. We have $Q_0 \sim -t/(2|\mathbf{K}|) \sim -t/T$ on the average. The mean energy loss in a single scattering is thus

$$\langle\Delta E\rangle_{1\,\mathrm{scat}} \sim \frac{1}{\sigma_{\mathrm{Coulomb}}}\int \mathrm{d}t\,\frac{\mathrm{d}\sigma_{\mathrm{Coulomb}}}{\mathrm{d}t}\,\frac{-t}{T} \sim \alpha T\ln\frac{|t|_{\max}}{\mu^2}. \tag{2.4}$$

The logarithm arises from the broad logarithmic interval $\mu^2 \ll |t| \ll |t|_{\max}$, implying (to logarithmic accuracy) that the energy transfer in a single collision is small compared to E.

Introducing the Coulomb mean free path,

$$\lambda_{\mathrm{Coulomb}} \equiv \frac{1}{n\sigma_{\mathrm{Coulomb}}} \sim \frac{1}{\alpha T}, \tag{2.5}$$

where $n \sim T^3$ is the particle density in the plasma, we estimate the energy loss rate per unit distance as

$$\frac{\mathrm{d}E_{\mathrm{Coulomb}}}{\mathrm{d}x} \sim \frac{\langle\Delta E\rangle_{1\,\mathrm{scat}}}{\lambda_{\mathrm{Coulomb}}} \sim \alpha^2 T^2 \ln\frac{|t|_{\max}}{\mu^2}. \tag{2.6}$$

The maximal transfer $|t|_{\max}$ is given by

$$|t|_{\max} = \frac{(s-M^2)^2}{s} \sim \begin{cases} ET, & M^2 \ll ET, \\ \dfrac{E^2T^2}{M^2}, & M^2 \gg ET, \end{cases} \tag{2.7}$$

where $s = (P+K)^2 = M^2 + 2PK$, and hence $s \sim ET$ in the domain of small masses and $s \sim M^2$ in the domain of large masses. We thus see that the logarithmic factor in (2.6) takes different forms in the mass domains $M^2 \ll ET$ and $M^2 \gg ET$,

$$\frac{\mathrm{d}E_{\mathrm{Coulomb}}}{\mathrm{d}x} \sim \alpha^2 T^2 \begin{cases} \ln\dfrac{ET}{\mu^2}, & M^2 \ll ET, \\ 2\ln\dfrac{ET}{\mu M}, & M^2 \gg ET. \end{cases} \tag{2.8}$$

Two remarks are in order here.

(1) Strictly speaking, using (2.2) for the differential cross section is not correct. First, it is written for static and scalar plasma particles, while the particles are moving and have spin. Second, the diagram in Fig. 2a was evaluated with the model expression $1/(t-\mu^2)$ for the photon propagator, while the actual expression is more involved. Third, neither the S-matrix nor the cross section is well defined in the medium, because there are no asymptotic states in the medium, and the relevant quantity is not σ^{tot} but the damping rate ζ of the ultrarelativistic collective excitation with the muon quantum numbers, related to the muon mean free path by $\lambda = \zeta^{-1}$. This damping rate was evaluated in Ref. [35], with the result[6]

$$\lambda = \zeta^{-1} = \left(\frac{1}{2}\,\alpha T\ln\frac{C}{\alpha}\right)^{-1}. \tag{2.9}$$

[5] Following the usage adopted in the literature on this subject, we use the word 'Coulomb' in a generalized sense, also including *screened Coulomb*, i.e., Yukawa.

[6] The calculation was done for QCD, but the Abelian result is directly obtained from the result for ζ_{q} by setting $c_F = 1$ in Ref. [35].

Thus, the mean free path involves an extra logarithm of the coupling constant compared to our estimate (2.5). This is because (2.9) depends on magnetic interactions in addition to Coulomb scattering [35, 36]. Hence, strictly speaking, it is (2.9) that should be taken as the definition of λ to be used in Sections 3–5. However, keeping track of the logarithms of the coupling constant is a difficult problem, which we do not address. The only logarithms we keep are those depending on the particle energy E. Hence, throughout our study, we use $\lambda \sim 1/(\alpha T)$, which coincides with the Coulomb mean free path in (2.5).

(2) A more standard way to define the mean free path is not as in (2.5) but $\lambda^{\rm tr} = 1/(n\sigma^{\rm tr})$, where

$$\sigma^{\rm tr} = \int {\rm d}\sigma\,(1-\cos\theta) \tag{2.10}$$

is the transport cross section involving an additional suppression factor for small-angle scattering. The transport mean free path $\lambda^{\rm tr}$ conveniently describes standard transport phenomena associated with collisions (viscosity, electric conductivity, etc.).[7] For the problem of collisional energy loss, the use of definition (2.10) is equally warranted when deriving (2.6) (the estimates for $\langle\Delta E\rangle_{1\,\rm scat}$ and λ would be different, but their ratio would not change). Scale (2.5) also appears not to be very physical in the problem of radiative losses. Almost all the results there depend not on λ as such but on the combination $\hat{q} = \mu^2/\lambda$, which is a transport coefficient. The 'isolated' scale λ only enters arguments of certain logarithms. We return to this point when concluding in Section 6. We only stress now that, irrespectively of whether it is observable, the notion of mean free path defined in (2.5) or (2.9) proves to be very convenient and instructive, and we use this definition throughout the paper.

We now turn to collisional losses due to Compton scattering (Fig. 2b), and focus on the region $M^2 \ll ET$. For $M^2 \ll |u| \ll s \sim ET$, the differential Compton scattering cross section is given by

$$\frac{{\rm d}\sigma_{\rm Compton}}{{\rm d}t} \sim \frac{\alpha^2}{su}\,. \tag{2.11}$$

This gives the total Compton cross section

$$\sigma_{\rm Compton} \sim \frac{\alpha^2}{s}\ln\frac{s}{M^2} \sim \frac{\alpha^2}{ET}\ln\frac{ET}{M^2}. \tag{2.12}$$

The logarithm occurs from the integration in the domain $M^2 \ll |u| \ll s \simeq |t|$ (recall that $s+t+u=2M^2$). Similarly to (2.4), we find the energy loss in a single Compton scattering as

$$\langle\Delta E\rangle_{1\text{ Compton scat}} \sim \frac{1}{\sigma_{\rm Compton}}\int {\rm d}t\,\frac{{\rm d}\sigma_{\rm Compton}}{{\rm d}t}\,\frac{-t}{T} \sim \frac{s}{T} \sim E. \tag{2.13}$$

Therefore, the characteristic energy transfer is of the order of E. (Experimental projects to produce energetic photons by scattering energetic electrons on laser beams are based on this property of Compton scattering [38].) Introducing the Compton mean free path

$$\lambda_{\rm Compton} \equiv \frac{1}{n\sigma_{\rm Compton}} \sim \frac{E}{\alpha^2 T^2 \ln(ET/M^2)} \gg \lambda_{\rm Coulomb}\,, \tag{2.14}$$

we obtain

$$\frac{{\rm d}E_{\rm Compton}}{{\rm d}x} \sim \frac{E}{\lambda_{\rm Compton}} \sim \alpha^2 T^2 \ln\frac{ET}{M^2}. \tag{2.15}$$

We note that the logarithm in (2.15) arises from the same logarithmic integral (over u) as for the total Compton cross section (2.12), and that it is present only in the mass domain $M^2 \ll ET$.

We see that losses due to the Coulomb and Compton scattering are of the same order, although the two processes differ drastically. Compton scattering is rare, $\lambda_{\rm Compton} \gg \lambda_{\rm Coulomb}$, but, as mentioned above, it is very efficient in transferring energy. Summing the Coulomb and Compton contributions to the collisional loss in the domain $M^2 \ll ET$, we obtain[8]

$$\left.\frac{{\rm d}E_{\rm coll}}{{\rm d}x}\right|_{\mu^-} = \frac{\pi}{3}\,\alpha^2 T^2\left[\ln\frac{ET}{\mu^2} + \frac{1}{2}\ln\frac{ET}{M^2} + \mathcal{O}(1)\right], \quad M^2 \ll ET. \tag{2.16}$$

In Compton scattering, when $M^2 \ll ET$, we have $|u| \ll s$ to the leading logarithmic accuracy, implying that $|t| \simeq |t|_{\max} \simeq s$. Therefore, in this mass region, Compton scattering is characterized by a final state consisting of a *soft* muon and a *hard* photon (of energy $\simeq E$) ejected from the plasma. This constitutes the main difference from the case of Coulomb scattering, where the leading (logarithmically enhanced) contribution to the cross section is made by processes with small energy transfer. But beyond the leading logarithmic approximation, the constant Coulomb and Compton contributions to ${\rm d}E/{\rm d}x$ are made by similar typical configurations, where the final muon and the scattered particle have almost equal shares of the initial energy E [33].

We finally note that for $M^2 \gg ET$, the Compton logarithm in (2.16) should be dropped, and the Coulomb logarithm is modified (see (2.8)), giving

$$\left.\frac{{\rm d}E_{\rm coll}}{{\rm d}x}\right|_{\mu^-} = \frac{2\pi}{3}\,\alpha^2 T^2\left[\ln\frac{ET}{\mu M} + \mathcal{O}(1)\right], \quad M^2 \gg ET. \tag{2.17}$$

2.1.2 Ultrarelativistic electron. At first sight, the collisional loss of an energetic electron crossing an e^+e^- plasma is given by (2.16) with the muon mass $M \gg \mu$ replaced by the electron thermal mass in the medium $m_{\rm th} \sim eT \sim \mu$. But as noted above, the leading Compton contribution corresponds to the situation where the incoming particle loses almost all its energy. Therefore, it seems impossible to distinguish the final soft electron from a thermal electron. In other words, when an energetic electron becomes soft after interacting with the plasma, it effectively disappears. In addition, the incoming electron can be annihilated with a thermal positron. A similar situation arises when discussing a positron energy loss in usual matter.

One way to better define an *observable* energy loss in this case is to require the final electron to be hard enough, e.g., to

[7] For a thorough discussion of transport phenomena in a QGP, see [37].

[8] See Ref. [33] for the exact calculation, where the constant beyond the logarithmic accuracy is also evaluated.

have the energy $E' > E/2$. Under this constraint, the final energetic electron cannot be confused with a thermal electron [the Fermi–Dirac thermal weight of electrons involves an exponential suppression, $n_F(E') \simeq \exp(-E'/T) \ll 1$ for $E' \gtrsim E/2 \gg T$]. Requiring the presence of an energetic electron in the final state allows discarding the annihilation channel, as well as the leading (logarithmic) Compton contribution. Only the Coulomb contribution, which to the logarithmic accuracy corresponds to small energy transfers, should be kept.

With this setup, we obtain

$$\left.\frac{\mathrm{d}E_{\mathrm{coll}}}{\mathrm{d}x}\right|_{e^-,\,E'\gtrsim E/2} = \frac{\pi}{3}\,\alpha^2 T^2\left[\ln\frac{ET}{\mu^2} + \mathcal{O}(1)\right] \tag{2.18}$$

from (2.16).

2.2 Quark–gluon plasma

2.2.1 Tagged heavy quark. Here, we consider the case of an ultrarelativistic heavy quark ($E \gg M \gg T$) crossing a QGP. For clarity, we focus on the limit $M^2 \ll ET$. (For $M^2 \gg ET$, as in QED, the Compton logarithm is to be dropped and the Coulomb logarithm modified; see (2.8).) The purely collisional energy loss does not depend much on the production mechanism of the heavy quark. This quark can be produced in a hard process within the medium (as in heavy-ion collisions) or preexist inside a heavy meson coming from infinity. The crucial difference between these two situations reveals itself when studying the radiative energy loss of a quark induced by its rescattering in the plasma.

The calculation of the heavy quark collisional loss in a QGP is similar to the case of a muon crossing an e^+e^- plasma. The main change consists in the running of the coupling α_s. This must be taken into account, not only to improve the accuracy of predictions but also to obtain the correct energy dependence of $\mathrm{d}E/\mathrm{d}x$.

The contribution to $\mathrm{d}E/\mathrm{d}x$ from the Coulomb scattering of a fast heavy quark on thermal quarks and gluons is easily inferred from the QED case. The Coulomb differential cross section is $\propto \alpha_s^2$, and the scale at which α_s must be evaluated is given by the invariant momentum transfer t itself. Due to the running of α_s, the logarithmic integral appearing in the fixed-coupling (QED) expression (2.4) is modified to [32]

$$\alpha^2\int_{\mu^2}^{ET}\frac{\mathrm{d}|t|}{|t|} \to \int_{\mu^2}^{ET}\frac{\mathrm{d}|t|}{|t|}\,\alpha_s^2(t)\,. \tag{2.19}$$

Using $\alpha_s(t) \sim 1/\ln(|t|/\Lambda^2)$, we can integrate the right-hand side of (2.19) exactly and rewrite it as

$$\alpha^2\ln\frac{ET}{\mu^2} \to \alpha_s(\mu^2)\,\alpha_s(ET)\ln\frac{ET}{\mu^2}. \tag{2.20}$$

A similar discussion applies to the contribution from Compton scattering on thermal gluons.[9] To the logarithmic accuracy, Compton scattering is dominated by the u-channel exchange. The relevant scale determining the coupling in the differential cross section for this contribution is of the order $\mathcal{O}(u)$. The total Compton scattering cross section in QCD is obtained from QED expression (2.12) by replacing

$$\alpha^2\int_{M^2}^{ET}\frac{\mathrm{d}|u|}{|u|} \to \int_{M^2}^{ET}\frac{\mathrm{d}|u|}{|u|}\,\alpha_s^2(u)\,. \tag{2.21}$$

In other words,

$$\alpha^2\ln\frac{ET}{M^2} \to \alpha_s(M^2)\,\alpha_s(ET)\ln\frac{ET}{M^2}. \tag{2.22}$$

Using (2.20) and (2.22) in (2.16), we obtain the fast heavy quark collisional loss in the limit $M^2 \ll ET$ (after performing the thermal average over the target quarks and gluons and introducing color factors [34]) as

$$\left.\frac{\mathrm{d}E_{\mathrm{coll}}}{\mathrm{d}x}\right|_{Q} = \frac{4\pi}{3}\,T^2\left[\left(1+\frac{n_f}{6}\right)\alpha_s(\mu^2)\,\alpha_s(ET)\ln\frac{ET}{\mu^2} + \frac{2}{9}\,\alpha_s(M^2)\,\alpha_s(ET)\ln\frac{ET}{M^2} + \mathcal{O}(\alpha_s^2)\right]. \tag{2.23}$$

The term beyond the logarithmic accuracy $\sim \mathcal{O}(\alpha_s^2)$ was found in Ref. [34]. Similarly to the QED case, the Compton leading logarithm in (2.23) corresponds to final state configurations with a soft (but *tagged*) heavy quark jet and a hard jet initiated by a gluon of energy $\simeq E$ knocked out of the plasma.[10]

2.2.2 (Untagged) light parton. Similarly to the case of QED, it would be misleading to pretend to obtain the energy loss of an energetic light parton by replacing the mass M in (2.23) by the light thermal parton mass $\sim gT$. First, even though this is not done in practice, it is theoretically possible to observe the events with a soft tagged heavy quark. But for a light (and hence untagged) parton, this is impossible. Second, light quarks may annihilate with light antiquarks in a heat bath, and this adds to the intrinsic uncertainty of what the energy loss of a light parton is.

As regards Compton scattering, the situation is even worse than in QED, where the detection of an energetic photon in the final state would at least signal that Compton scattering had occurred. In QCD, it is very difficult to distinguish the hadron jet initiated by a hard final gluon produced in Compton scattering from the hadron jet initiated by a hard final quark having undergone soft Coulomb exchanges.

For a light (or, more generally, untagged) parton, the *observable* energy loss must be defined, at the partonic level, with respect to the leading (i.e., most energetic) parton. When $E' < E/2$, or equivalently $|u| < s/2$, the corresponding energy loss is $\Delta E = E - |\mathbf{K}'| = E' - |\mathbf{K}| \simeq E' \sim |u|/(2|\mathbf{K}|)$. When $E' > E/2$, we have $\Delta E = E - E' \sim |t|/(2|\mathbf{K}|)$, as in the case of a tagged parton. The Compton contribution to $\mathrm{d}E/\mathrm{d}x$ therefore has the form

$$\frac{\mathrm{d}E_{\mathrm{Compton}}}{\mathrm{d}x} \sim n\int_{M^2}^{s}\mathrm{d}|u|\,\frac{\alpha_s^2}{s|u|}\left[\frac{|u|}{T}\,\Theta\left(\frac{s}{2}-|u|\right) + \frac{|t|}{T}\,\Theta\left(|u|-\frac{s}{2}\right)\right]. \tag{2.24}$$

[9] In QCD, the terms *Coulomb* and *Compton* refer not to different processes, as they do in QED, but to different kinematical regions associated with the same process. The amplitude $\mathcal{M}(\mathrm{Qg}\to\mathrm{Qg})$ is dominated by the Coulomb diagram with a soft gluon exchange when $|t|$ is small. The same amplitude is dominated by a Compton-like diagram corresponding to the u-channel exchange when $|u|$ is small.

[10] We note that such configurations are presently not counted in the RHIC experimental setup, due to a lower energy cut-off used in the selection of heavy quark tagged events. Under those experimental conditions, only the Coulomb leading logarithm should be kept in (2.23).

We note that in contrast to the 'tagged' case, the Compton contribution has no logarithmic enhancement. The reason is clear: the logarithm $\ln(ET/M^2)$ in (2.23) came from the small u region. But with the 'untagged' physical definition in (2.24), small u corresponds to small energy transfer, and does not make any important (logarithmic) contribution to the energy loss. With such a definition, we also note that the annihilation channel contribution does not yield any logarithm either.

Thus, as regards the leading logarithms, we are left with only the t-channel Coulomb logarithm arising from the broad interval $\mu^2 \ll |t| \ll ET$. This Coulomb logarithm can be inferred from (2.23). The generalization to the gluon case is obvious, and we obtain

$$\left.\frac{\mathrm{d}E_{\mathrm{coll}}}{\mathrm{d}x}\right|_{\mathrm{q,g}} = C_{\mathrm{R}}\pi T^2\left[\left(1+\frac{n_{\mathrm{f}}}{6}\right)\alpha_{\mathrm{s}}(\mu^2)\,\alpha_{\mathrm{s}}(ET)\ln\frac{ET}{\mu^2}+\mathcal{O}(\alpha_{\mathrm{s}}^2)\right], \tag{2.25}$$

with $C_{\mathrm{R}} = 4/3$ (3) being the quark (gluon) color charge. Replacing $\alpha_{\mathrm{s}}(\mu^2)\alpha_{\mathrm{s}}(ET) \to \alpha_{\mathrm{s}}^2$ in (2.25), we recover the fixed-α_{s} Bjorken result in (2.1). We stress that Bjorken's result is valid in the logarithmic approximation and is specific to the untagged experimental setup.

3. Radiative loss of a fast asymptotic charged particle. QED

We now discuss the radiative energy loss due to bremsstrahlung. In this section, we consider the case of an *asymptotic* charged particle (i.e., produced in the remote past) crossing a finite-size plasma layer. This is a natural experimental setup in QED, where it is possible to prepare an on-shell energetic electron entering the plasma with its already formed proper field 'coat.' We therefore consider the QED case first. In Section 4, we study the somewhat academic but instructive case of an 'asymptotic quark' crossing a QGP.

3.1 Fast electron

Here, we evaluate the radiative energy loss of an on-shell energetic electron going through an ultrarelativistic $\mathrm{e}^+\mathrm{e}^-$ plasma. We assume that $E \gg T$ and $\mu \sim eT \gg m$, where $m \equiv m_{\mathrm{e}}$ is the electron mass. The electron is scattered by the plasma particles, changes the direction of its motion, and emits bremsstrahlung photons.

***L* ≪ *λ*: Bethe–Heitler regime.** We first consider the case of a very thin plasma layer of size $L \ll \lambda$, where the electron mean free path λ is the characteristic distance between subsequent elastic scatterings.[11] As discussed in Section 2, λ is given by (2.9), or rather by (2.5), because we neglect logarithms of the coupling constant in our study. The probability that the incoming electron undergoes Coulomb scattering is $\sim L/\lambda \ll 1$, and the probability of having several scatterings is further suppressed. The average energy loss after crossing the length L is thus

$$\Delta E(L \ll \lambda) \sim \frac{L}{\lambda}\,\Delta E_{\mathrm{1\,scat}}^{\mathrm{rad}}\,, \tag{3.1}$$

where $\Delta E_{\mathrm{1\,scat}}^{\mathrm{rad}}$ is the radiative energy loss induced by a single Coulomb scattering.[12] It is obtained from the photon radiation spectrum derived by calculating the two diagrams in Fig. 3,

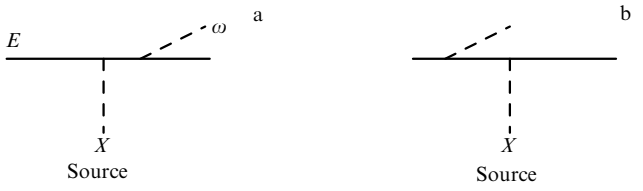

Figure 3. The two diagrams for photon radiation induced by the electron Coulomb scattering.

$$\Delta E_{\mathrm{1\,scat}}^{\mathrm{rad}} = \int \frac{\mathrm{d}I_{\mathrm{rad}}}{\mathrm{d}\omega}\,\omega\,\mathrm{d}\omega\,. \tag{3.2}$$

The result for the radiation spectrum does not depend much on the nature of scatterers. It depends mainly on the characteristic scattering cross section and hence on the characteristic momentum transfer $q_\perp$. As is argued in what follows, the Compton scattering plays virtually no role here, and we can consider only the Coulomb scatterings. Therefore, we can replace the plasma particles by static sources and use form (2.2) for the differential cross section. The integral giving the total Coulomb cross section in (2.3) is saturated by the values $|t| \simeq q_\perp^2 \sim \mu^2$ and, in most estimates (with the few exceptions to be considered in what follows), we can assume $q_\perp$ to be of the order of the Debye mass μ.

In the soft-photon approximation $\omega = |\mathbf{k}| \ll E$, which is sufficient for our purposes,[13] the photon radiation intensity is given by

$$\mathrm{d}I_{\mathrm{rad}} = \sum_{i=1,2} e^2\left|\frac{P\varepsilon_i}{Pk}-\frac{P'\varepsilon_i}{P'k}\right|^2\frac{\mathrm{d}^3\mathbf{k}}{(2\pi)^3 2\omega}\,, \tag{3.3}$$

where ε_i are two transverse photon polarization vectors. When the photon radiation 'angle' $\boldsymbol{\theta} \equiv \mathbf{k}_\perp/\omega$ and the electron scattering 'angle' $\boldsymbol{\theta}_{\mathrm{s}} \equiv \mathbf{q}_\perp/E$ are small, $\theta, \theta_{\mathrm{s}} \ll 1$, the sum over photon polarizations gives

$$\mathrm{d}I_{\mathrm{rad}} = \frac{\alpha}{\pi^2}\,\frac{\mathrm{d}\omega}{\omega}\,\mathrm{d}^2\boldsymbol{\theta}\,\mathbf{J}_{\mathrm{e}}^2\,, \tag{3.4}$$

$$\mathbf{J}_{\mathrm{e}} = \frac{\boldsymbol{\theta}'}{\theta'^2+\theta_{\mathrm{m}}^2}-\frac{\boldsymbol{\theta}}{\theta^2+\theta_{\mathrm{m}}^2}\,, \tag{3.5}$$

$$\mathbf{J}_{\mathrm{e}}^2 = \frac{\theta_{\mathrm{s}}^2}{(\theta^2+\theta_{\mathrm{m}}^2)(\theta'^2+\theta_{\mathrm{m}}^2)}-\left(\frac{\theta_{\mathrm{m}}}{\theta^2+\theta_{\mathrm{m}}^2}-\frac{\theta_{\mathrm{m}}}{\theta'^2+\theta_{\mathrm{m}}^2}\right)^2, \tag{3.6}$$

where $\theta_{\mathrm{m}} \equiv m/E$ and $\boldsymbol{\theta}' \equiv \boldsymbol{\theta} - \boldsymbol{\theta}_{\mathrm{s}}$.

We are interested in the small-mass and large-mass limits, respectively corresponding to $\theta_{\mathrm{m}} \ll \theta_{\mathrm{s}}$ and $\theta_{\mathrm{m}} \gg \theta_{\mathrm{s}}$. We then

[11] In this paper, L denotes the distance traveled by the particle in the plasma, to be distinguished from the plasma size L_{p}. For thermal equilibration to occur, the size of the medium should be much larger than the *transport* mean free path of plasma particles (which is of the same order as the transport mean free path of an energetic electron), $L_{\mathrm{p}} \gg \lambda^{\mathrm{tr}} \sim 1/(\alpha^2 T) \gg \lambda$. Thus, the situation $L \ll \lambda$, implying $L \ll L_{\mathrm{p}}$, is quite unrealistic for an asymptotic electron, for which we expect $L \sim L_{\mathrm{p}}$, unless the electron is crossing the plasma near its edge. (The limit $L \ll \lambda$ is somewhat more meaningful in the case of particles produced within a plasma, which we considered in Section 5.) However, in order to better understand what happens in the more physical situation with larger L, we find it instructive to first consider the case $L \ll \lambda$.

[12] The radiative energy losses induced by a single scattering is referred to as Bethe–Heitler losses in this paper.

[13] In fact, the characteristic frequency of emitted photons contributing to ΔE_{rad} is of the order of E (see, e.g., spectrum (3.9) below). But this modifies the result obtained in the soft-photon approximation only by numerical factors, which is not our concern here.

have

$$\theta_{\rm m} \ll \theta_{\rm s} \Rightarrow \int \frac{{\rm d}^2\boldsymbol{\theta}}{2\pi}\, \mathbf{J}_{\rm e}^2 \simeq \ln\frac{\theta_{\rm s}^2}{\theta_{\rm m}^2} \Rightarrow \omega\,\frac{{\rm d}I_{\rm rad}}{{\rm d}\omega} \simeq \frac{2\alpha}{\pi}\ln\frac{\theta_{\rm s}^2}{\theta_{\rm m}^2}, \quad (3.7)$$

$$\theta_{\rm m} \gg \theta_{\rm s} \Rightarrow \int \frac{{\rm d}^2\boldsymbol{\theta}}{2\pi}\, \mathbf{J}_{\rm e}^2 \simeq \frac{1}{3}\frac{\theta_{\rm s}^2}{\theta_{\rm m}^2} \Rightarrow \omega\,\frac{{\rm d}I_{\rm rad}}{{\rm d}\omega} \simeq \frac{2\alpha}{3\pi}\frac{\theta_{\rm s}^2}{\theta_{\rm m}^2}\,. \quad (3.8)$$

Equation (3.7) is valid to the logarithmic accuracy. The logarithm arises from the first term in (3.6) and from the angular regions $\theta_{\rm m} \ll \theta \ll \theta_{\rm s}$ and $\theta_{\rm m} \ll \theta' = |\boldsymbol{\theta} - \boldsymbol{\theta}_{\rm s}| \ll \theta_{\rm s}$. Asymptotic expressions (3.7) and (3.8) are conveniently incorporated into the following interpolating formula for the energy spectrum,

$$\omega\,\frac{{\rm d}I_{\rm rad}}{{\rm d}\omega} = \frac{2\alpha}{\pi}\int\frac{{\rm d}^2\boldsymbol{\theta}}{2\pi}\,\mathbf{J}_{\rm e}^2 \simeq \frac{2\alpha}{\pi}\ln\left(1+\frac{\theta_{\rm s}^2}{3\theta_{\rm m}^2}\right) \sim \alpha\ln\left(1+\frac{q_\perp^2}{3m^2}\right). \quad (3.9)$$

The exact expression displays the same qualitative behavior, but is more complicated [39].

When $q_\perp \sim \mu \gg m$ (implying $\theta_{\rm s} \gg \theta_{\rm m}$), we obtain

$$\Delta E_{1\,\rm scat}^{\rm rad} \sim \int^E \frac{{\rm d}I_{\rm rad}}{{\rm d}\omega}\,\omega\,{\rm d}\omega \sim \alpha E\ln\frac{\mu^2}{m^2}, \quad (3.10)$$

and for the Bethe–Heitler (BH) energy loss per unit distance,

$$\frac{{\rm d}E_{\rm BH}}{{\rm d}x}\,(L \ll \lambda) \sim \frac{\Delta E_{1\,\rm scat}^{\rm rad}}{\lambda} \sim \alpha^2 ET\ln\frac{\mu^2}{m^2}. \quad (3.11)$$

We now discuss a possible modification of this result due to Compton scattering. Essentially, there is none. (This is in contrast to the collisional loss. We have seen in Section 2 that the contributions due to the Compton and Coulomb scattering are of the same order there.) Indeed, for Compton scattering, $\Delta E_{1\,\rm scat}^{\rm rad}$ is of the same order as for Coulomb scattering, $\Delta E_{1\,\rm scat}^{\rm rad} \sim \alpha E$, but the corresponding mean free path (2.14) is much larger and

$$\frac{{\rm d}E_{\rm Compton}^{\rm rad}}{{\rm d}x}\,(L \ll \lambda) \sim \frac{\alpha E}{\lambda_{\rm Compton}} \sim \alpha^3 T^2 \quad (3.12)$$

is much smaller than the BH contribution in (3.11) induced by Coulomb scattering. Compton contribution (3.12) is even smaller than collisional loss (2.18), and is not mentioned any more in this paper.

We see that when $L \ll \lambda$, the BH radiative loss of an energetic electron crossing an ultrarelativistic plasma, Eqn (3.11), is much larger than its collisional loss (2.18),

$$L \ll \lambda \Rightarrow \frac{{\rm d}E_{\rm BH}}{{\rm d}E_{\rm coll}} \sim \frac{E}{T} \gg 1\,. \quad (3.13)$$

It is instructive to compare this with the energy losses of an ultrarelativistic particle in usual matter [1], consisting of nonrelativistic electrons and static nuclei. The basic difference between usual matter and the e^+e^- plasma is that screening effects do not play an important role in the former. Certainly, the electric fields of individual electrons and nuclei are screened at atomic distances $\sim 1/(\alpha m)$, but these are comparatively large distances (see the footnote below). Screening in usual matter can affect the arguments of certain logarithms, but is otherwise unimportant for order-of-magnitude estimates. In the following digression on usual matter, we neglect logarithms.

We first consider collisional losses. Weighing the $e^-e^- \to e^-e^-$ Coulomb differential cross section ${\rm d}\sigma/{\rm d}t \sim \alpha^2/t^2$ with the energy transfer $\Delta E(t)$, we obtain

$$\left(\frac{{\rm d}E}{{\rm d}x}\right)_{\rm coll}^{\rm usual\ matter} \sim nZ\int\frac{\alpha^2}{t^2}\,\Delta E(t)\,{\rm d}t\,, \quad (3.14)$$

where n is the number of atoms per unit volume and Z is the number of electrons in an atom. Using $t = -2KQ \simeq -2(mQ_0 - \mathbf{KQ})$, we have $Q_0 = \Delta E(t) \simeq |t|/(2m)$. We obtain, up to some logarithm,

$$\left(\frac{{\rm d}E}{{\rm d}x}\right)_{\rm coll}^{\rm usual\ matter} \sim \frac{nZ\alpha^2}{m}\,. \quad (3.15)$$

We note that the order of magnitude of the collisional energy loss in a hot plasma is recovered from (3.15) by replacing $Z \to 1$, $n \to T^3$, and $m \to T$.

We next discuss radiative losses. We assume (as we also did for a hot plasma) that the matter layer is thin enough, such that $\Delta E(L) \ll E$. In addition, we first assume the scattered energetic particle to be an electron and the medium to be hydrogen ($Z = 1$). Then the radiative losses due to scattering by electrons and nuclei (protons) are of the same order. When $q_\perp \ll m$, the characteristic energy loss in a single scattering is $\sim \alpha E$ times the suppression factor $\sim q_\perp^2/m^2 \simeq |t|/m^2$ [see (3.8)]. Hence, instead of (3.14) and (3.15), we obtain the BH radiative loss in the form

$$\left(\frac{{\rm d}E}{{\rm d}x}\right)_{\rm BH}^{\rm hydrogen} \sim n\int\frac{\alpha^2}{t^2}\,(\alpha E)\,\frac{|t|}{m^2}\,{\rm d}|t| \sim \frac{n\alpha^3 E}{m^2}\,. \quad (3.16)$$

Neglecting logarithms, estimate (3.11) for radiative losses in an ultrarelativistic (thin) plasma is obtained from (3.16) by replacing $n \to T^3$ and $m \to \mu \sim eT$, instead of $m \to T$ as in the case of collisional losses.[14]

In cold hydrogen, the characteristic ratio of radiative and collisional losses is

$$\frac{{\rm d}E_{\rm BH}}{{\rm d}E_{\rm coll}} \sim \frac{\alpha E}{m}\,, \quad (3.17)$$

with an additional suppression factor α compared to (3.13) due to the different screening properties of plasma and usual matter. That is why radiative losses in usual matter dominate only at relatively high energies $E \gg m/\alpha$. For electrons in hydrogen, the critical energy where the radiative and collisional losses are equal is $E_{\rm c} \sim 350$ MeV [40].

The physics of collisional and radiative losses differ in one important respect. The energetic particle loses a tiny fraction of its energy in a collision with an individual electron, much like a cannon ball loses a tiny fraction of its energy in a collision with an individual air molecule. The drag force ${\rm d}p/{\rm d}t = {\rm d}E/{\rm d}x$ is an adequate physical quantity to describe this. On the other hand, about half of the original particle energy is lost during a single radiation act. Estimate (3.16) refers to an *average* drag force, but the fluctuations of this

[14] This can be understood by noting that in the plasma case, because of screening at the scale μ, only the region $|t| \gtrsim \mu^2 \gg m^2$ contributes. (In usual matter, screening occurs at some scale $|t|_{\rm min} \ll m^2$.) Therefore, the factor $|t|/m^2$ in (3.16) disappears and the t-integral is saturated by $|t| \sim \mu^2$.

quantity are very large. That is why radiative losses are usually described not in terms of drag force (3.16) but in terms of the radiation length X_0, the average distance at which about half of the energy (more precisely, the fraction $1 - 1/\mathrm{e}$) is lost. This is especially sensible if we recall that $-\mathrm{d}E_{\mathrm{BH}}/\mathrm{d}x \propto E$ and the energy therefore decreases exponentially.

We see in what follows that although the radiative energy losses of light partons passing a QCD plasma strongly fluctuate for the same reason as electron radiative losses occur, the notion of radiation length is not very reasonable there because the linear BH law in (3.16) does not hold and the energy dependence of $\mathrm{d}E/\mathrm{d}x$ is more complicated. Anticipating the discussion in what follows, we also note that the radiation spectrum of sufficiently heavy quarks (but not of heavy Abelian charged particles!) turns out to be soft, and hence the physics is more similar to the physics of collisional loss and the drag force fluctuations are suppressed.

When $Z > 1$ and the incoming particle is heavy, $M \gg m$, two new effects become relevant. First, radiation mainly occurs when the incoming particle is scattered on a heavy nucleus, due to the enhancement factor Z^2 (the nucleus charge squared) compared to the cross section in hydrogen. The collisional loss is still due to scattering on electrons and involves only the factor Z (the number of electrons in an atom). Second, the radiation intensity is suppressed at small momentum transfers by the factor $\sim q_\perp^2/M^2$. We obtain

$$\frac{\mathrm{d}E_{\mathrm{BH}}}{\mathrm{d}E_{\mathrm{coll}}} \sim \frac{Z\alpha Em}{M^2} \,. \tag{3.18}$$

The suppression factor $q_\perp^2/M^2 \sim \mu^2/M^2$ is also effective for radiative losses of a massive particle passing through an ultrarelativistic QED plasma [see (3.8) and (3.37)]. The meaning of the condition $\mu \sim eT \gg m$ imposed at the beginning of the section now becomes clear. When $\mu \gg M$, a particle of mass M passing through a plasma can be considered light. When $M \gg \mu$, it can be considered heavy, and its radiative loss in a QED plasma is suppressed, at least for $L \ll \lambda$ [see (3.37) below] by the factor $\sim \mu^2/M^2$.[15]

***L* ≫ *L**: LPM regime.** After this digression, we return to the case of a hot plasma and consider a medium of a very large size. Estimate (3.1) is correct for small $L \ll \lambda$, the factor L/λ bearing the meaning of the electron scattering *probability*. At first sight, this estimate can be extended to the region $L \gg \lambda$, with the factor L/λ interpreted as the *number* of electron scatterings, but this is not correct because the basic assumption underlying the derivation of (3.1) — that one photon is emitted in each scattering — is invalid here.

Indeed, the radiation process takes time. The particle is not ready to radiate again until its accompanying radiation field coat is formed. Strictly speaking, it takes an infinite time for the coat to be fully developed such that the particle can be treated as an asymptotic state. But if we are interested only in the emission of photons in a particular wave-vector range, we are not obliged to wait forever and should only ensure that the corresponding Fourier harmonics of the radiation field are already present in the coat. The length at which a harmonic corresponding to radiation of the photon of a frequency ω at an angle θ is formed, the *formation length*, is given by[16]

$$\ell_{\mathrm{f}}(\omega,\theta) \sim \frac{E}{\kappa^2} \simeq \frac{1}{\omega\theta^2} \simeq \frac{\omega}{k_\perp^2} \,, \tag{3.19}$$

where $\kappa^2 \simeq 2E\omega(1-\cos\theta) \simeq E\omega\theta^2$ is the virtuality of the internal electron in Fig. 3a.

The formation length $\sim 1/(\omega\theta^2)$ can be interpreted as the length at which a photon of the energy ω emitted at an angle θ acquires a phase of the order of unity in the frame comoving with the particle. The last condition is, indeed,

$$\begin{aligned} \langle\text{phase disbalance}\rangle &\sim \omega t - k_\parallel \ell \\ &\sim \ell\Big(\omega - \sqrt{\omega^2 - \omega^2\theta^2}\,\Big) \sim \ell\omega\theta^2 \sim 1 \,, \end{aligned} \tag{3.20}$$

where we assume that the electron moves with the speed of light, $t = \ell$ (this can be done because $k_\perp \simeq \omega\theta \gg m$).

The crucial observation is that even if the electron is scattered *several* times before traveling the distance $\ell_{\mathrm{f}}(\omega,\theta)$, it cannot emit (to the leading order in α) more than *one* photon with the energy ω at the angle θ. Indeed, in this case, we cannot speak about independent photon emissions, and we are dealing with coherent emission of a single photon in a multiple scattering process. As a result, photon emission with $\ell_{\mathrm{f}}(\omega,\theta) \gg \lambda$ is suppressed compared to the situation where it would be additive in the number of elastic scatterings. This is known as the Landau–Pomeranchuk–Migdal (LPM) effect [23–25].

At fixed ω and for $\mu \gg m$, radiation spectrum (3.9) induced by a single scattering arises from the angular domains $\theta_{\mathrm{m}} \ll \theta \ll \theta_{\mathrm{s}}$ and $\theta_{\mathrm{m}} \ll \theta' \equiv |\boldsymbol{\theta} - \boldsymbol{\theta}_{\mathrm{s}}| \ll \theta_{\mathrm{s}}$, i.e., from the formation lengths

$$\frac{E^2}{\omega\mu^2} \ll \ell_{\mathrm{f}}(\omega,\theta) \ll \frac{E^2}{\omega m^2} \,. \tag{3.21}$$

In the integrated spectrum, we have $\omega \sim E$, and therefore BH radiative loss (3.11) arises from the photon formation lengths

$$\frac{E}{\mu^2} \ll \ell_{\mathrm{f}}(E,\theta) \ll \frac{E}{m^2} \,. \tag{3.22}$$

For $E \gg T$, we have $E/\mu^2 \gg \lambda$, and therefore the radiated photons contributing to the BH loss in (3.11) are formed far away from the medium layer of size $L \ll \lambda$.

What happens when the medium size increases, that is, $L \gg \lambda$? Using the estimate E/μ^2 for the typical formation length of radiated photons (which was obtained for a *thin* medium with a size $L \ll \lambda$), we would naively expect the energy loss to be approximately given by $\Delta E^{\mathrm{rad}}_{1\,\mathrm{scat}}$ in (3.10) up to the scale $L \sim E/\mu^2$, with the entire medium acting as a *single* effective scattering center. But this is not so. The critical size L^* beyond which $\Delta E(L)$ strongly differs from $\Delta E^{\mathrm{rad}}_{1\,\mathrm{scat}}$ happens to be much smaller than E/μ^2. It is approximately given by the geometric mean of λ and E/μ^2,

$$\lambda \ll L^* \sim \sqrt{\frac{\lambda E}{\mu^2}} \sim \frac{1}{\alpha T}\sqrt{\frac{E}{T}} \ll \frac{E}{\mu^2} \,. \tag{3.23}$$

[15] This suppression, which, as can be inferred from (3.8), is due to the suppression of radiation in the cone $\theta < \theta_M \equiv M/E$, is sometimes called the *dead cone* effect [26].

[16] For our purposes, it is better to speak about the formation length rather than the formation time. In the rest frame of the virtual electron, the formation time/length is of the order of $1/\sqrt{\kappa^2}$. In the laboratory frame, it is multiplied by the Lorentz factor $E/\sqrt{\kappa^2}$. In general, the angle θ entering (3.19) is the angle between the photon and the electron from which it is radiated (the final electron in Fig. 3a).

To find how this scale arises, we consider the limit $L \to \infty$. In this case, all radiated photons are formed in the medium, and the estimate of the typical photon formation length $\ell_{\rm f}^{\rm med}$ is modified compared to the case of the vacuum. To see this, we substitute the typical electron deviation angle $\theta_{\rm s}^2$ at the length $\ell_{\rm f}^{\rm med}$ for θ^2 in estimate (3.19),

$$\ell_{\rm f}^{\rm med} \sim \frac{1}{\omega\theta_{\rm s}^2(\ell_{\rm f}^{\rm med})} \sim \frac{1}{\omega N\mu^2/E^2}\,, \tag{3.24}$$

where $N = \ell_{\rm f}^{\rm med}/\lambda$ is the number of electron scatterings on the distance $\ell_{\rm f}^{\rm med}$. The last estimate in (3.24) relies on the Brownian motion picture, namely, on the assumption that the transverse momentum transfers in successive elastic scatterings are not correlated. We obtain

$$\ell_{\rm f}^{\rm med}(\omega) \sim \sqrt{\frac{\lambda E^2}{\omega\mu^2}}\,. \tag{3.25}$$

Substituting $\omega \sim E$, we thus obtain estimate (3.23) for the characteristic in-medium formation length L^*.

Scattering centers located within the distance $\sim L^*$ act as one effective scattering center, inducing a *single* photon radiation act. For $L \gg L^*$, the medium contains L/L^* effective scattering centers, and the estimate of the radiative energy loss is obtained as this number times the energy lost in a single photon radiation act,[17]

$$\Delta E(L \gg L^*) \sim \alpha E\,\frac{L}{L^*} \sim \alpha L\sqrt{\frac{\mu^2}{\lambda}\,E} \sim \alpha^2 L\sqrt{ET^3}\,. \tag{3.26}$$

This estimate was obtained under the assumption that the typical momentum transfer squared after N electron scatterings is $q_\perp^2(N) \sim N\mu^2$ (μ being the typical transfer in one scattering). In fact, this is correct only when the $q_\perp$-distribution in a single elastic scattering decreases rapidly enough at large $q_\perp$, such that the average $\langle q_\perp^2\rangle$ is well defined. But for Coulomb scattering, the integral

$$\langle q_\perp^2\rangle = \int {\rm d}q_\perp^2\, q_\perp^2\,\frac{\mu^2}{(q_\perp^2+\mu^2)^2} \tag{3.27}$$

diverges logarithmically as the ultraviolet cut-off $q_\perp^2\big|_{\rm max} \sim |t|_{\rm max} \sim ET \to \infty$. It can be shown (see Ref. [14] or Appendix A for an alternative derivation) that the typical transfer after N Coulomb scatterings scales as $(N\ln N)\,\mu^2$ instead of $N\mu^2$. The presence of this logarithm somewhat modifies the estimate of L^* in (3.23), but otherwise does not affect the above heuristic derivation. We thus find

$$L^* \sim \sqrt{\frac{\lambda E}{\mu^2\ln(L^*/\lambda)}} \sim \sqrt{\frac{\lambda E}{\mu^2\ln\bigl(E/(\lambda\mu^2)\bigr)}}\,, \tag{3.28}$$

$$\Delta E(L \gg L^*) \sim \alpha E\,\frac{L}{L^*} \sim \alpha^2 L\sqrt{ET^3\,\ln\frac{E}{T}}\,. \tag{3.29}$$

[17] This energy is given by (3.10), but *without* the mass-dependent logarithmic factor. This is because our estimate $\ell_{\rm f}^{\rm med} \sim L^*$ displays no logarithmic spread, contrarily to (3.22). This can also be expressed [using (3.19)] by noting that the electron traveling in the medium is off the mass shell, with a characteristic virtuality of the order of $\kappa_{\rm med}^2 \sim E/L^* \sim \sqrt{E\mu^2/\lambda} \sim \alpha\sqrt{ET^3}$. This is in contrast to the logarithmic spread $m^2 \ll \kappa^2 \ll \mu^2$ in the vacuum.

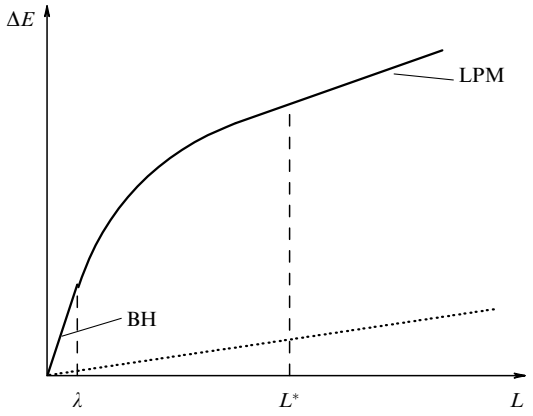

Figure 4. Schematic plot of the radiative energy loss of an asymptotic light ($m \ll \mu$) and fast ($E \gg T$) charged particle crossing a hot e^+e^- plasma, as functions of the distance L traveled by the particle in the plasma. The dotted line represents the collisional energy loss $\Delta E_{\rm coll}(L) \sim \alpha^2 T^2 L$.

The parameter dependence of this last result agrees with that found in Ref. [41]. At both small $L \ll \lambda$ [see (3.1)] and large $L \gg L^*$ [see (3.29)], the radiative energy loss is proportional to L. But the proportionality coefficients in those two regions are different. At large L, the slope is smaller as a result of the LPM suppression. The behavior of $\Delta E(L)$ is represented schematically in Fig. 4.

It is worth noting that for $L \gg L^*$, the in-medium *energy spectrum* of the radiated photons can be easily obtained from (3.25),

$$\omega\,\frac{{\rm d}I_{\rm rad}}{{\rm d}\omega}(L) \sim \alpha\,\frac{L}{\ell_{\rm f}^{\rm med}(\omega)} \sim \alpha\sqrt{\frac{\omega\,\omega_{\rm c}}{E^2}}, \qquad \omega > \frac{E^2}{\omega_{\rm c}}\,, \tag{3.30}$$

where we introduce the energy scale

$$\omega_{\rm c} \sim \frac{L^2\mu^2}{\lambda}\,. \tag{3.31}$$

With the correct logarithmic factor included as discussed above, spectrum (3.30) is given by

$$\omega\,\frac{{\rm d}I_{\rm rad}}{{\rm d}\omega}(L) \sim \alpha^2 L\sqrt{\frac{\omega}{E^2}\,T^3\,\ln\frac{E^2}{\omega T}}\,. \tag{3.32}$$

Integrating this spectrum over ω up to $\omega \sim E$, we recover (3.29). The LPM suppression is more pronounced at low ω, where the photon formation length in (3.25) is larger.

In the case of usual matter, the LPM effect was observed experimentally for energetic electrons crossing thin metal foils, first at SLAC [42] and more recently at the CERN SPS [43]. An accurate description of the data based on rigorous theoretical calculations is available [24, 44].

Intermediate region $\lambda \ll L \ll L^*$. The region $\lambda \ll L \ll L^*$ is transitional between the BH and LPM regimes. The energy loss in this region is the same as that induced by a single effective scattering with the typical momentum transfer $q_\perp^2(N) \sim (N\ln N)\,\mu^2$, where $N = L/\lambda$. The energy loss is estimated similarly to (3.10):

$$\Delta E(\lambda \ll L \ll L^*) \sim \alpha E\,\ln\left(\frac{L}{\lambda}\,\frac{\mu^2}{m^2}\right). \tag{3.33}$$

This estimate is associated with the photon formation lengths

$$\frac{E}{\mu^2 L/\lambda} = \ell_{\rm f}\big|_{\rm min} \ll \ell_{\rm f} \ll \frac{E}{m^2} \tag{3.34}$$

[cf. (3.22)]. Result (3.33) holds because the radiated photon 'sees' only one effective scattering center, i.e., $\ell_{\rm f}\big|_{\rm min} \gg L$. This condition is precisely equivalent to $L \ll L^*$.

The regimes $L \ll \lambda$ and $\lambda \ll L \ll L^*$ smoothly match when $L \sim \lambda$ [see (3.11) and (3.33)]. Comparing (3.33) and (3.29), we now see that the former estimate of $\Delta E(L = L^*)$ involves an extra logarithmic factor and dominates at this point. It is associated with photons radiated outside the medium. Adding the LPM linear term (3.29) to (3.33), we obtain

$$\Delta E(L \gtrsim L^*) \sim \alpha E \ln\left(\frac{L^*}{\lambda}\frac{\mu^2}{m^2}\right) + \alpha E \frac{L}{L^*}\,. \tag{3.35}$$

The linear regime sets in when the second term starts to dominate. This occurs at the scale

$$L \sim L^* \ln\left(\frac{L^*}{\lambda}\frac{\mu^2}{m^2}\right), \tag{3.36}$$

which is somewhat larger than L^*.

3.2 Energetic muon

What happens if the ultrarelativistic particle going through the plasma is heavy, i.e., $M \gg \mu \sim eT$? As already mentioned, the intensity of the BH radiation for massive charged particles is suppressed by the factor $\sim \mu^2/M^2$ [see (3.8)]. For $L \ll \lambda$, we therefore have

$$\Delta E(L \ll \lambda) \sim \alpha E \frac{L}{\lambda}\frac{\mu^2}{M^2} \sim \frac{\alpha^3 T^3 E}{M^2}\, L\,. \tag{3.37}$$

The suppression factor $\sim \mu^2/M^2$ in (3.8) arises from an integral over the photon radiation angle of the type

$$\theta_{\rm s}^2 \int_{\theta_M^2} \frac{{\rm d}\theta^2}{\theta^4} \sim \frac{\theta_{\rm s}^2}{\theta_M^2}\,, \tag{3.38}$$

which is saturated by the angles $\theta^2 \sim \theta_M^2 \equiv M^2/E^2$.

We note that for a massive particle, expression (3.19) for the vacuum formation length is modified,

$$\ell_{\rm f}(\omega,\theta) \to \ell_{\rm f}(\omega,\theta,M) \sim \frac{1}{\omega(\theta^2+\theta_M^2)}\,. \tag{3.39}$$

The characteristic formation length of emitted photons is therefore of the order of

$$\ell_{\rm f}^{\rm heavy} \sim \frac{1}{\omega\theta_M^2} \sim \frac{E}{M^2}\,. \tag{3.40}$$

If $M^2 \ll \alpha ET$, then $\ell_{\rm f}^{\rm heavy} \gg \lambda \gg L$, i.e., the photons are mostly formed outside the medium.

We now consider the behavior of the radiative energy loss for larger lengths. There are two distinct cases, depending on whether M^2 is smaller or larger than $\alpha\sqrt{ET^3}$. The appearance of this scale is easy to understand from our previous study of the light-particle case. We showed, in particular, that the result in (3.26) (or, more accurately, (3.29)) in the domain $L \gg L^*$ corresponds to the electron in-medium virtuality of the order of $\kappa_{\rm med}^2 \sim \alpha\sqrt{ET^3}$. We thus expect strong modifications of $\Delta E(L)$ compared to the light-particle case, when $M^2 \gg \alpha\sqrt{ET^3}$, and milder modifications when $M^2 \ll \alpha\sqrt{ET^3}$.

(A) $M^2 \ll \alpha\sqrt{ET^3}$. The condition $M^2 \ll \alpha\sqrt{ET^3}$ is equivalent to the condition that formation length (3.40) exceed the scale L^* given in (3.23) or (3.28),

$$\frac{E}{M^2} \gg L^* \sim \sqrt{\frac{\lambda E}{\mu^2}} \Leftrightarrow M^2 \ll \sqrt{\frac{\mu^2 E}{\lambda}} \sim \alpha\sqrt{ET^3}\,. \tag{3.41}$$

When L somewhat exceeds λ, the medium still acts as a single effective scattering center, transferring the momentum $q_\perp^2 \sim (L/\lambda)\mu^2$ to the massive particle. The energy loss is given by αE times the suppression factor $q_\perp^2/M^2 \sim (L/\lambda)(\mu^2/M^2)$ because $q_\perp^2/M^2 \ll 1$. The result *coincides* with (3.37), which is therefore valid as L increases up to the scale L^{**} defined by

$$L^{**} \equiv \lambda\frac{M^2}{\mu^2} \gg \lambda\,. \tag{3.42}$$

Hence, we can write

$$\Delta E(L \ll L^{**}) \sim \alpha E \frac{L}{\lambda}\frac{\mu^2}{M^2} \sim \frac{\alpha^3 T^3 E}{M^2}\, L\,. \tag{3.43}$$

As soon as the suppression factor disappears, the problem reduces to the already discussed case of light particles. Vacuum formation length (3.40) is modified in the medium to L^*. For large lengths $L \gg L^*$, the dependence of ΔE on L is linear with the same slope as for light particles,

$$\Delta E(L \gg L^*) \sim \alpha E \frac{L}{L^*}\,. \tag{3.44}$$

As for a light particle, we can infer that in the intermediate region $L^{**} \ll L \ll L^*$, we have [see (3.33)]

$$\Delta E(L^{**} \ll L \ll L^*) \sim \alpha E \ln\left(\frac{L}{\lambda}\frac{\mu^2}{M^2}\right) \sim \alpha E \ln\frac{L}{L^{**}}. \tag{3.45}$$

The overall behavior is displayed by the solid line in Fig. 5. It is similar to the case of a light particle (see Fig. 4), with the scale L^{**} playing the role of λ. We also note the relation

$$L^* = \sqrt{L^{**}\,\ell_{\rm f}^{\rm heavy}}\,, \tag{3.46}$$

which is analogous to (3.23).

(B) $M^2 \gg \alpha\sqrt{ET^3}$. This case corresponds to formation length (3.40) being smaller than L^*,

$$\frac{E}{M^2} \ll L^* \Leftrightarrow M^2 \gg \alpha\sqrt{ET^3}\,. \tag{3.47}$$

If the vacuum formation length in (3.40) is less than the would-be in-medium formation length L^*, then the LPM effect never plays a role. The linear law in (3.37) is valid for *all* lengths. Indeed, it naturally extends up to the scale $L = E/M^2$, where the suppression factor $(L/\lambda)(\mu^2/M^2) \sim L/L^{**}$ is still present. As L increases further, the suppression factor stays frozen, but the number of emitted photons increases,

$$\Delta E\left(L \gg \frac{E}{M^2}\right) \sim \frac{L}{E/M^2}\left(\frac{E/M^2}{L^{**}}\right)\alpha E \sim \alpha E \frac{L}{\lambda}\frac{\mu^2}{M^2}\,. \tag{3.48}$$

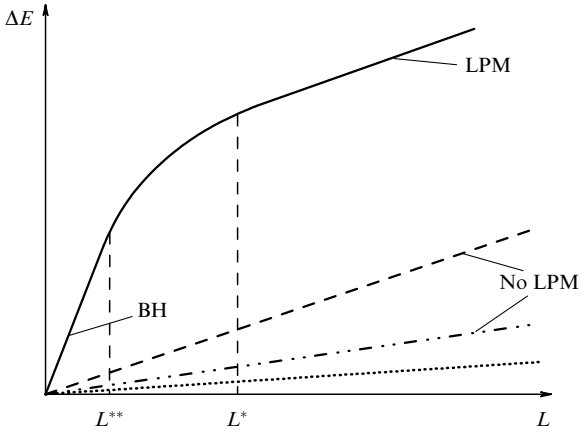

Figure 5. Radiative energy loss of a heavy charged QED particle. Solid line: moderately heavy particle, $\mu^2 \sim \alpha T^2 \ll M^2 \ll \alpha\sqrt{ET^3}$. Dashed line: $M^2 \sim \alpha\sqrt{ET^3}$. Dash-dotted line: $M^2 \gg \alpha\sqrt{ET^3}$. Dotted line: collisional loss.

This coincides with (3.37). The behavior of $\Delta E(L)$ in this case is represented by the dash-dotted curve in Fig. 5.

We summarize the results in this section by briefly discussing the different slopes that appear in Figs 4 and 5. We consider a fixed energy E and progressively increase the particle mass. When the particle is light (see Fig. 4), the slope for $L \ll \lambda$ is larger than the slope for $L \gg L^*$ by the factor $\sqrt{E/T}$. As the mass increases (see Fig. 5, solid line), the linear regime at small L extends to L^{**} (instead of λ) and has a slope reduced by the factor μ^2/M^2. This slope is still larger than the slope at $L \gg L^*$ as long as $M^2 \ll \alpha\sqrt{ET^3}$. When $M^2 \sim \alpha\sqrt{ET^3}$ (see Fig. 5, dashed line), L^{**} coincides with L^*, the two slopes also coincide, and $\Delta E(L)$ is given by (3.37) for all L. As M increases further (see Fig. 5, dash-dotted line), $\Delta E(L)$ is still given by (3.37); in particular, its slope decreases as $\sim 1/M^2$.

Comparing this slope with the slope $\sim \alpha^2 T^2$ for the collisional energy loss (see Section 2), we see that the radiative losses of a massive QED particle parametrically dominate over collisional ones (dotted line in Fig. 5) when the mass is not too large or, equivalently, at large enough energies:

$$M^2 \ll \alpha ET \Leftrightarrow E \gg \frac{M^2}{\alpha T}\,. \tag{3.49}$$

This condition for the dominance of radiative losses in a QED plasma is actually equivalent to the vacuum formation length $\ell_{\rm f}^{\rm heavy} \sim E/M^2$ being larger than the mean free path λ. It is also interesting to note that (3.49) can be put in correspondence with energy losses (3.15) and (3.18) of a massive particle crossing usual matter with the replacements $Z \to 1$, $m \to T$, and $n \to T^3$.

4. Radiative loss of an 'asymptotic parton'

An experiment where an incoming energetic parton (constituent of an asymptotic hadron) enters a preexisting QGP, suffers radiative energy loss, and then escapes the QGP is, unfortunately, not feasible. We nevertheless regard the problem of evaluating the radiative loss of such an 'asymptotic parton' crossing a QGP as an instructive and useful theoretical exercise. We spend some time on it before passing to the more realistic case of a parton produced in a medium in Section 5.

The problem of the energy loss of a parton coming from infinity is somewhat better posed (at the level of a thought experiment at least) for a tagged heavy quark than for a light parton. When the quark is heavy (i.e., when the quark mass satisfies the condition $M \gg \Lambda_{\rm QCD}$), we can think, as was discussed in the Introduction, of a heavy meson (or heavy baryon) scattering in a thermos bottle containing the QGP. The heavy-quark energy loss in the QGP is roughly the same as the energy difference between the initial heavy meson and the final fast hadron with the same flavor.

If the projectile is a light meson (e.g., a pion), it contains at least two light valence quarks, and the energy loss of a single quark in the QGP is unobservable because of the absence of tagging. We can still imagine a thought experiment where the net energy loss of the light projectile constituents passing through some medium could be observed. We consider the situation where the two valence quarks of the incoming pion materialize as two separate jets after crossing the medium. For the jets to be well separated, they should have a large relative transverse momentum. This can happen if the pion enters the medium in a compact configuration (i.e., with a large relative transverse momentum between the quarks) and loses coherence due to in-medium rescatterings. Although the sum of the total energies of the final jets should coincide with the initial pion energy, the energy loss of light quarks after the pion dissociation should affect the energy distribution of the *leading hadrons* within the jets. The pion diffractive dissociation process in cold nuclear matter, $\pi + A \to 2\,\text{jets} + A$, has been studied experimentally [45] as a tool to access the pion wave function [46]. The light-quark energy loss in nuclear matter should in principle affect this process. A similar experiment with a QGP can be considered. Therefore, the energy loss of an 'asymptotic light parton' crossing a QGP is observable *in principle*.

In what follows, we study the cases of both light and heavy partons, with a parton considered *light* if its mass is less than the Debye mass $\mu \sim gT$ in a QGP, and *heavy* otherwise. We assume that $\mu \gg \Lambda_{\rm QCD}$, and hence, with this definition, a light parton ($m \ll \mu$) can also be heavy in the usual sense ($m \gg \Lambda_{\rm QCD}$). We follow the same reasoning as in QED (see Section 3) and study the behavior of the radiative loss in different regions of the distance L traveled by a colored particle.

4.1 Light parton

We consider the case of a light quark rather than of a gluon, since it is technically more convenient (we also discuss heavy quarks, and it is instructive to see what changes as the mass increases). In the following formulas, the parameter m stands for the quark mass when $\Lambda_{\rm QCD} \ll m \ll \mu$, but should be replaced with $\Lambda_{\rm QCD}$ if the quark is actually light in the usual sense, $m \lesssim \Lambda_{\rm QCD}$. All the results for a gluon are qualitatively the same as for a light quark, with the replacement $m \to \Lambda_{\rm QCD}$ and with modified color factors (but those are not our concern in this paper).

***L* ≪ λ: Bethe–Heitler regime.** For $L \ll \lambda$, it is sufficient to determine the radiative loss induced by one scattering, as in (3.1). The gluon radiation amplitude $\mathcal{M}_{\rm rad}$ induced by a single elastic scattering also includes, besides the diagrams in Fig. 3 (with proper color factors), the diagram with the three-

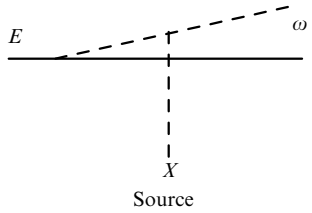

Figure 6. The diagram with a three-gluon vertex contributing to the third term in (4.1).

gluon vertex shown in Fig. 6. This diagram is evaluated, for instance, in Ref. [47] for a massless quark. The generalization to a massive quark is trivial and for $\omega \ll E$ (we work consistently in this approximation, as we did in QED), the sum of the three diagrams gives

$$\mathcal{M}_{\rm rad} \propto \left(\frac{\boldsymbol{\theta}}{\theta^2+\theta_{\rm m}^2}\, t^a t^b - \frac{\boldsymbol{\theta}'}{\theta'^2+\theta_{\rm m}^2}\, t^b t^a - \frac{\boldsymbol{\theta}''}{\theta''^2+\theta_{\rm m}^2} [t^a, t^b] \right) \boldsymbol{\varepsilon}\,. \tag{4.1}$$

In this expression, the parameters $\boldsymbol{\theta} = \mathbf{k}_\perp/\omega$, $\boldsymbol{\theta}' = \boldsymbol{\theta} - \boldsymbol{\theta}_{\rm s} = \boldsymbol{\theta} - \mathbf{q}_\perp/E$, and $\theta_{\rm m} = m/E$ are the same as in (3.5). We also set $\boldsymbol{\theta}'' = \boldsymbol{\theta} - \boldsymbol{\theta}_{\rm g}$, with $\boldsymbol{\theta}_{\rm g} = \mathbf{q}_\perp/\omega$. The parameter $\theta_{\rm g}$ can be interpreted as the scattering angle of the virtual gluon with the energy $\simeq \omega$ in Fig. 6. The color factors can be conveniently grouped in terms of the commutator $[t^a, t^b]$ and anticommutator $\{t^a, t^b\}$ of color matrices. Equation (4.1) can then be rewritten as

$$\mathcal{M}_{\rm rad} \propto \left[[t^a, t^b] \left(\mathbf{J}_{\rm q} - \frac{1}{2}\, \mathbf{J}_{\rm e} \right) + \{t^a, t^b\}\, \frac{1}{2}\, \mathbf{J}_{\rm e} \right] \boldsymbol{\varepsilon}\,, \tag{4.2}$$

where $\mathbf{J}_{\rm e}$ [already given in (3.5)] and $\mathbf{J}_{\rm q}$ are given by

$$\mathbf{J}_{\rm e} = \frac{\boldsymbol{\theta}'}{\theta'^2+\theta_{\rm m}^2} - \frac{\boldsymbol{\theta}}{\theta^2+\theta_{\rm m}^2}\,, \tag{4.3}$$

$$\mathbf{J}_{\rm q} = \frac{\boldsymbol{\theta}''}{\theta''^2+\theta_{\rm m}^2} - \frac{\boldsymbol{\theta}}{\theta^2+\theta_{\rm m}^2}\,. \tag{4.4}$$

The soft-gluon radiation intensity can be obtained by squaring (4.2), summing/averaging over color indices, and normalizing by the elastic scattering cross section. For $N_{\rm c}$ quark colors, we obtain

$$\begin{aligned} {\rm d}I_{\rm rad} &= \frac{\alpha_{\rm s}}{\pi^2}\, \frac{{\rm d}\omega}{\omega}\; {\rm d}^2\boldsymbol{\theta} \left[N_{\rm c} \left(\mathbf{J}_{\rm q} - \frac{1}{2}\, \mathbf{J}_{\rm e} \right)^2 + \frac{N_{\rm c}^2-2}{N_{\rm c}} \left(\frac{1}{2}\, \mathbf{J}_{\rm e} \right)^2 \right] \\ &= \frac{\alpha_{\rm s}}{\pi^2}\, \frac{{\rm d}\omega}{\omega}\; {\rm d}^2\boldsymbol{\theta} \left\{ N_{\rm c}\, \mathbf{J}_{\rm q}^2 - \frac{1}{2N_{\rm c}}\, \mathbf{J}_{\rm e}^2 + \frac{N_{\rm c}}{2} \left[(\mathbf{J}_{\rm q} - \mathbf{J}_{\rm e})^2 - \mathbf{J}_{\rm q}^2 \right] \right\}. \end{aligned} \tag{4.5}$$

In the second expression, the terms are organized so as to facilitate the integration over angles. Considering a light quark with $m \ll \mu$ and using (3.7), we see that the first term in the right-hand side of (4.5) contributes to the energy spectrum as

$$\omega\, \frac{{\rm d}I_{\rm rad}}{{\rm d}\omega}\bigg|_{\rm broad} \sim \alpha_{\rm s} \ln \frac{\theta_{\rm g}^2}{\theta_{\rm m}^2} \sim \alpha_{\rm s} \ln \left(\frac{\mu^2}{m^2}\, \frac{E^2}{\omega^2} \right), \tag{4.6}$$

the logarithm arising from the *broad* angular domain $\theta_{\rm m} \ll \theta \ll \theta_{\rm g}$. The second term is similar to the one in the QED case [see (3.4)]. Its contribution to the spectrum is

$$\omega\, \frac{{\rm d}I_{\rm rad}}{{\rm d}\omega}\bigg|_{\rm narrow} \sim \alpha_{\rm s} \ln \frac{\theta_{\rm s}^2}{\theta_{\rm m}^2} \sim \alpha_{\rm s} \ln \frac{\mu^2}{m^2}\,, \tag{4.7}$$

arising from the *narrow* angular domain $\theta_{\rm m} \ll \theta \ll \theta_{\rm s}$. The third term in the right-hand side of (4.5) does not bring any logarithm into the energy spectrum and is neglected in what follows. Integrating (4.6) and (4.7) over ω, we see that the terms $\propto \mathbf{J}_{\rm q}^2$ and $\propto \mathbf{J}_{\rm e}^2$ contribute similarly to the radiative loss,[18]

$$\Delta E_{\rm 1\,scat}^{\rm rad} \sim \alpha_{\rm s} E \ln \frac{\mu^2}{m^2}\,. \tag{4.8}$$

Thus, in the case of a light quark, $m \ll \mu$, we have

$$\Delta E(L \ll \lambda) \sim \frac{L}{\lambda}\, \Delta E_{\rm 1\,scat}^{\rm rad} \sim \alpha_{\rm s} E\, \frac{L}{\lambda} \ln \frac{\mu^2}{m^2} \tag{4.9}$$

similarly to the QED case [see (3.1) and (3.10)].

To recapitulate, at a fixed $\omega \ll E$, we have $\theta_{\rm s} \ll \theta_{\rm g}$, and the differential energy spectrum receives two logarithmic contributions: a QED-like contribution from the narrow region $\theta_{\rm m} \ll \theta \ll \theta_{\rm s}$ and a contribution specific to QCD from the broad region $\theta_{\rm m} \ll \theta \ll \theta_{\rm g}$. The second contribution (which dominates at large $N_{\rm c}$) is given by

$$\omega\, \frac{{\rm d}I_{\rm rad}}{{\rm d}\omega}\bigg|_{\rm broad} \sim \alpha_{\rm s} \int {\rm d}^2\boldsymbol{\theta}\, \mathbf{J}_{\rm q}^2\,. \tag{4.10}$$

Using that $\mathbf{k}_\perp \simeq \omega\boldsymbol{\theta}$ and neglecting the quark mass, we can write spectrum (4.10) as

$$\omega\, \frac{{\rm d}I_{\rm rad}}{{\rm d}\omega\, {\rm d}^2\mathbf{k}_\perp}\bigg|_{k_\perp \gg\, \omega\mu/E} \sim \alpha_{\rm s}\, \frac{q_\perp^2}{k_\perp^2 (\mathbf{k}_\perp - \mathbf{q}_\perp)^2}\,, \tag{4.11}$$

which is the well-known Gunion–Bertsch spectrum [47].

We emphasize that spectrum (4.10) is obtained from QED spectrum (3.4) by replacing the electron scattering angle $\theta_{\rm s} \equiv q_\perp/E \sim \mu/E$ with the virtual gluon scattering angle $\theta_{\rm g} \equiv q_\perp/\omega \sim \mu/\omega$ [cf. (4.3) and (4.4)]. This fact has interesting consequences.

(1) At a fixed $\omega \ll E$, the broad angular domain $\theta_{\rm m} \ll \theta \ll \theta_{\rm g}$ contributing to (4.10) translates into the interval in gluon formation lengths

$$\frac{\omega}{\mu^2} \ll \ell_{\rm f}(\omega) \ll \frac{E^2}{\omega m^2}\,, \tag{4.12}$$

which can be compared to the corresponding interval (3.21) in the case of QED. Therefore, in QCD, the gluon starts to be formed at much shorter lengths

$$\ell_{\rm f}(\omega)\Big|_{\rm min} \sim \frac{\omega}{\mu^2} \tag{4.13}$$

than the photon in QED. Because $\ell_{\rm f}(\omega)\big|_{\rm min} \propto \omega$ in QCD, we expect the LPM suppression of energy loss to *increase* with increasing ω [in QED, the opposite was true; see the remark after (3.32)]. We discuss this in more detail below.

[18] This is because we have $\omega \sim E$ in the integrated spectrum, and the broad and narrow angular domains then coincide.

(2) Because $\omega \sim E$ in the *integrated* spectrum (in which case the broad QCD domain $\theta \ll \theta_g$ coincides with the narrow QED domain $\theta \ll \theta_s$), the typical formation lengths in QED and QCD are in the same range [see (3.22)],

$$\frac{E}{\mu^2} \ll \ell_f(\omega \sim E) \ll \frac{E}{m^2}\,. \tag{4.14}$$

We hence anticipate that the average radiative loss of a light quark has a parameter dependence similar to that of an electron for all travel distances L.

(3) On the other hand, if the characteristic frequencies ω in the integrated spectrum are much smaller than E, then the broad angular domain is indeed broader than the narrow one, and we obtain different parametric behaviors for the radiative loss in QCD and QED. We see in Section 4.2 that this is exactly what happens for heavy quarks.

***L* ≫ *L**: LPM regime.** The derivation of the light quark energy loss for $L \gg L^*$ follows the same lines as in QED, with some differences discussed below. First, for $L \gg L^*$, similarly to the photon case, a single gluon is emitted in a multiple scattering process composed of $N \sim \ell_f^{\rm med}(\omega)/\lambda$ individual scatterings. This amounts to exchanging N gluons in the t channel. This N-gluon state can be either a color octet or a color singlet (higher representations do not contribute to the quark scattering amplitude). In the color singlet case, the physics is the same as in QED, and the radiated gluon is emitted within a narrow cone[19] with the angle $\theta_s^2(N) \sim N\mu^2/E^2$. For the color octet, the physics is the same as for the process with one gluon exchange discussed above involving two cones, but with the narrow and broad cone angles now being of the order of $\theta_s^2(N) \sim N\mu^2/E^2$ and $\theta_g^2(N) \sim N\mu^2/\omega^2$, respectively. In the large-N_c limit, the probability of having a singlet t-channel N-gluon state is suppressed by $1/N_c^2$ compared to the probability of having an octet. This suppression is of the same order as the suppression of the Abelian contribution yielding the narrow radiation cone in a single-gluon exchange [the second term in (4.5)]. In other words, the dynamics of gluon emission in a multiple scattering process is roughly the same as for single scattering, the only difference being that the characteristic momentum transfer μ^2 is multiplied by the factor $N \sim \ell_f^{\rm med}(\omega)/\lambda$.

The in-medium gluon formation length $\ell_f^{\rm med}(\omega)$ is obtained from (3.19) by replacing the gluon radiation angle θ^2 with $\theta_g^2(N) \sim N\mu^2/\omega^2$:

$$\ell_f^{\rm med}(\omega) \sim \frac{\omega}{N\mu^2} \Rightarrow \ell_f^{\rm med}(\omega) \sim \sqrt{\frac{\omega\lambda}{\mu^2}}\,. \tag{4.15}$$

The gluon formation length increases with ω, the opposite behavior compared to QED [see (3.25)]. The gluons with $\omega \sim E$ are formed within the length L^* given in (3.23), leading to the same parameter dependence of the radiative loss as in QED:

$$\Delta E(L \gg L^*) \sim \alpha_s E \frac{L}{L^*} \sim \alpha_s L \sqrt{\frac{\mu^2}{\lambda} E} \sim \alpha_s^2 L \sqrt{ET^3}\,. \tag{4.16}$$

However, there are differences between the dynamics of energy losses by an electron and a light quark.

(1) Similarly to QED, due to the long tail in the Coulomb scattering potential, the typical transverse momentum exchange $q_{\rm typ}^2(N)$ after N scatterings is not exactly $N\mu^2$. As shown in Appendix A, it is $q_{\rm typ}^2 \sim (N \ln N)\,\mu^2$ in QED, but in QCD this simple dependence is replaced by (A.25) due to the running of α_s. For very large N, $q_{\rm typ}^2(N)$ is given by expression (A.26), which does not involve the factor $\ln N$. This means that the factor $\sim \sqrt{\ln E}$ in the energy loss of energetic light partons in the large-L region disappears for asymptotically large energies $\ln(E/T) \gg \ln(\mu/\Lambda_{\rm QCD})$. Instead of (3.28) and (3.29), we then have

$$L^* \sim \sqrt{\frac{\lambda E}{\mu^2 \ln \mu/\Lambda_{\rm QCD}}}\,, \tag{4.17}$$

$$\Delta E(L \gg L^*) \sim \alpha_s E \frac{L}{L^*} \sim \alpha_s^2 L \sqrt{ET^3 \ln \frac{\mu}{\Lambda_{\rm QCD}}}\,. \tag{4.18}$$

When the energy is large but not asymptotically large, the dependence is more complicated:

$$\Delta E(L \gg L^*) \sim \alpha_s^2 L \sqrt{ET^3 \frac{\alpha_s\bigl(\mu^2\sqrt{E/(\lambda\mu^2)}\,\bigr)}{\alpha_s(\mu^2)} \ln \frac{E}{T}}\,. \tag{4.19}$$

(2) Because of the difference between the gluon and photon formation lengths in (4.15) and (3.25), the gluon energy spectrum is not described by (3.30) but is given by

$$\omega \frac{{\rm d}I_{\rm rad}}{{\rm d}\omega}(L) \sim \alpha_s \frac{L}{\ell_f^{\rm med}(\omega)} \sim \alpha_s \sqrt{\frac{\omega_c}{\omega}}\,, \qquad \omega > \lambda\mu^2\,, \tag{4.20}$$

where ω_c is still given by (3.31), but now depends on the parameters μ and λ appropriate for a non-Abelian plasma. As expected, the LPM suppression in QCD increases with increasing ω, contrarily to QED. We note that below $\lambda\mu^2$, the formation length is less than λ and we are in the incoherent BH regime where the spectrum is given by (4.6) times the number of rescatterings L/λ.

Inserting the logarithmic factor discussed above, we obtain

$$\omega \frac{{\rm d}I_{\rm rad}}{{\rm d}\omega}(L) \sim \alpha_s^2 L \sqrt{\frac{T^3}{\omega} \ln \frac{\mu}{\Lambda_{\rm QCD}}}\,, \tag{4.21}$$

where we assume that $\ln(\omega/T) \gg \ln(\mu/\Lambda_{\rm QCD})$ [otherwise, the expression is more complicated, similarly to (4.19)].

Intermediate region $\lambda \ll L \ll L^*$. In this region, the analysis for an electron in Section 3.1 can be carried over directly to the QCD case of a light quark, yielding the result

$$\Delta E(\lambda \ll L \ll L^*) \sim \alpha_s E \ln\left(\frac{L}{\lambda}\frac{\mu^2}{m^2}\right). \tag{4.22}$$

As in the QED case, the result in (4.22) corresponds to the medium acting as a single effective scattering center. The medium size dependence enters only through the total momentum transfer $q_\perp^2 \sim (N \ln N)\,\mu^2$, where $N = L/\lambda$.

Equation (4.22) represents the so-called *factorization term* noted previously in Refs [12, 13, 15, 41]. Although the main goal of Ref. [15] was to address the radiative loss of a quark produced in a plasma, it is mentioned there that in the case of an 'asymptotic quark' entering the medium, the factorization term can be dropped when calculating the *induced* energy loss. As a consequence, the result in Ref. [15] for ΔE in the region $\lambda \ll L \ll L^*$ is $\Delta E \propto \alpha_s\omega_c$, instead of (4.22). But for an asymptotic quark, there is actually no distinction between

[19] In contrast to what happens in the BH regime, this cone does not produce any logarithmic factor [see footnote [17]].

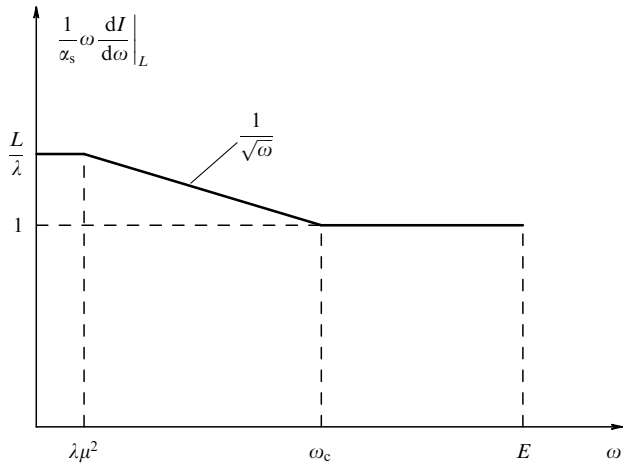

Figure 7. The gluon radiation spectrum of an asymptotic light quark crossing a hot QCD medium of size L, with $\lambda \ll L \ll L^*$ (double logarithmic plot).

the induced and the total radiative energy loss,[20] and factorization term (4.22) should be kept. Although the factorization term has a weak (logarithmic) dependence on L, it actually dominates over the term calculated in [15]. Indeed, for $L \ll L^*$, we have $\alpha_s\omega_c \ll \alpha_s E$.

To illustrate this point, we show the gluon radiation spectrum in the region $\lambda \ll L \ll L^*$ in Fig. 7. For $L \ll L^*$, we have $\omega_c \sim L^2\mu^2/\lambda \ll E$, and the spectrum is given by (4.20) or (4.21) in the interval $\lambda\mu^2 \ll \omega \ll \omega_c$. As mentioned above, for $\omega \ll \lambda\mu^2$, the spectrum is given by (4.6) times L/λ. For $\omega \gg \omega_c$, the gluon formation time is larger than L, and the spectrum is the same as for a single effective scattering, i.e., it is again obtained from (4.6) by replacing $\mu^2 \to \mu^2 L/\lambda$. This flat part of the spectrum makes the dominant contribution to the light-quark energy loss [see (4.22)].

Hence, the law $\Delta E(\lambda \ll L \ll L^*) \propto L^2$ [13–15, 17] for the induced energy loss of a light quark produced in a medium (we review this case in Section 5) is not valid for an asymptotic quark. Combining (4.9), (4.22), and (4.16), we see that the average radiative loss of an asymptotic light quark is similar to that of an asymptotic electron crossing a QED plasma. It is shown in Fig. 4.

4.2 Heavy quark

We have found that the radiative energy loss of an asymptotic light quark crossing a QGP has the same parameter dependence (apart from a logarithmic factor when $L \gg L^*$) as for an electron crossing a hot e^+e^- plasma, despite drastically different radiation spectra in these two cases. We see in what follows that the heavy-quark radiative loss is *different* from the heavy-muon loss in QED, and has a richer parameter dependence. The non-Abelian dynamics manifests itself more clearly for a heavy than for a light quark radiative energy loss.

We first consider the BH regime, $L \ll \lambda$.

For heavy quarks, $M \gg \mu$, the gluon radiation intensity is suppressed, similarly to the case of heavy leptons in QED. However, in the non-Abelian case, the suppression (dead cone effect) is not so strong because soft gluons are emitted in a cone broader than in QED [see (4.10) and the related discussion]. Estimate (3.9) for the QED radiation spectrum should be replaced with

$$\omega\,\frac{dI_{rad}}{d\omega}\bigg|_{1\,scat} \sim \alpha_s\int d^2\boldsymbol{\theta}\,\mathbf{J}_q^2 \sim \alpha_s \ln\left(1+\frac{\theta_g^2}{\theta_M^2}\right) \sim \alpha_s \ln\left(1+\frac{\mu^2}{M^2}\,\frac{E^2}{\omega^2}\right). \tag{4.23}$$

Integrating this spectrum over ω and multiplying by the scattering probability L/λ, we obtain

$$\Delta E(L \ll \lambda) \sim \alpha_s E\,\frac{L}{\lambda}\,\frac{\mu}{M} \sim \frac{g^5T^2E}{M}\,L\,. \tag{4.24}$$

Hence, for $L \ll \lambda$, the radiative loss of an asymptotic heavy quark is suppressed by the factor $\sim \mu/M$ instead of $\sim \mu^2/M^2$ in the QED case [see (3.37)].

A very important distinction between QCD and QED is that spectrum (4.23) of a heavy quark is soft. Indeed, the characteristic energy of emitted gluons is $\omega_{char} \sim \mu E/M \ll E$, and the spectrum decreases rapidly (as $1/\omega^2$) beyond this scale. (In contrast, the photon radiation spectrum of a heavy charged particle remains flat: mass effects result in a uniform suppression $\sim \mu^2/M^2$ for all ω.) Result (4.24) arises from small gluon energies, $\omega \sim \omega_{char}$. The typical gluon angles contributing to (4.24) are of the order of $\theta_{char}^2 \sim \theta_g^2 \sim \mu^2/\omega_{char}^2 \sim \theta_M^2$. Hence, the characteristic gluon formation length is

$$\ell_f^{\text{QCD heavy}} \sim \frac{1}{\omega_{char}\,\theta_{char}^2} \sim \frac{\omega_{char}}{\mu^2} \sim \frac{E}{\mu M}\,. \tag{4.25}$$

Similarly to the Abelian case, the behavior of the radiative loss at larger lengths depends on the ordering of different length scales: the mean free path λ, the characteristic formation length, or the scale L^{**} where the suppression $\sim \mu/M$ disappears. The ordering of these scales depends on the heavy-quark mass. In the Abelian case, we had two mass regions (3.41) and (3.47). In the non-Abelian case, there are three distinct regions.

(A) $M^2 \ll \alpha_s\sqrt{ET^3}$. In this case, the smallest length scale is $\lambda \sim 1/(\alpha_s T)$. For $L \ll \lambda$, law (4.24) holds. When L exceeds λ, the energy loss can be represented as being induced by one effective scattering with the momentum transfer $\mu_{eff}^2 \sim (L/\lambda)\mu^2$,

$$\Delta E(L) \sim \alpha_s E\,\frac{\mu\sqrt{L/\lambda}}{M} \sim \frac{\alpha_s^2 E\sqrt{LT^3}}{M}\,. \tag{4.26}$$

This law is valid in the region

$$\lambda \ll L \ll L^{**} = \lambda\,\frac{M^2}{\mu^2} \sim \frac{M^2}{\alpha_s^2T^3}\,. \tag{4.27}$$

At the scale L^{**}, the suppression $\sim \mu_{eff}/M$ disappears and the physics becomes the same as for light quarks. When L exceeds L^{**} but is less than the in-medium formation length L^* given by (4.17), there is still one effective scattering, and we are in the intermediate region. When $L \gg L^*$, the number of effective scatterings increases as L/L^*, and the radiative loss

[20] This is because an 'asymptotic on-shell quark' does not radiate in the absence of a medium. This is in contrast to a quark produced in a hard subprocess, which radiates even in the vacuum (see Section 5 for a further discussion of this point).

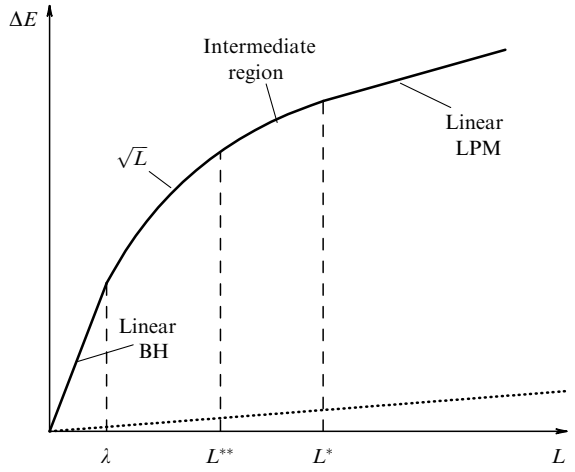

Figure 8. Radiative energy loss of an asymptotic heavy quark with $M^2 \ll \alpha_s\sqrt{ET^3}$. (Dotted line: collisional loss.)

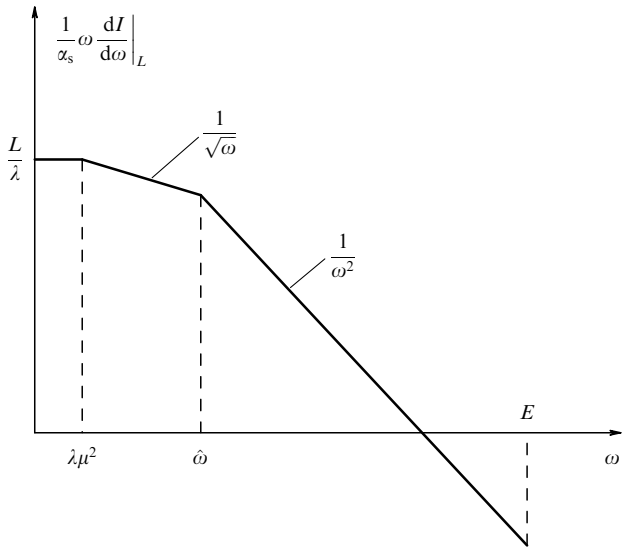

Figure 9. The gluon radiation spectrum of a heavy quark produced in a hot QGP for $\alpha_s\sqrt{ET^3} \ll M^2 \ll \alpha_s E^2$ and for $L \gg \tilde{L}^*$.

is given by the light-quark estimate in (4.18). A schematic plot of the energy dependence is shown in Fig. 8.

(B) $\alpha_s\sqrt{ET^3} \ll M^2 \ll \alpha_s E^2$. When M^2 exceeds $\alpha_s\sqrt{ET^3}$, the scale L^* becomes smaller than the scale L^{**} where the dead cone suppression disappears. Before proceeding, we note that the estimate $L^* \sim \sqrt{\lambda E/\mu^2}$ for the in-medium formation length no longer holds in this case, and L^* should be replaced with another scale $\tilde{L}^*$.

Indeed, we recall that the in-medium formation length is defined by the condition that it coincides with the vacuum formation length for an effective scattering with the transfer $\mu_{\rm eff}^2 \sim (L/\lambda)\,\mu^2$. For a light quark, this condition is given by

$$L \sim \frac{E}{\mu_{\rm eff}^2} \Rightarrow L^* \sim \sqrt{\frac{\lambda E}{\mu^2}}. \tag{4.28}$$

For a massive quark, the vacuum formation length is given by (4.25), and hence

$$L \sim \frac{E}{\mu_{\rm eff} M} \Rightarrow \tilde{L}^* \sim \left(\frac{\lambda E^2}{\mu^2 M^2}\right)^{1/3} \sim \left(\frac{L^{*4}}{L^{**}}\right)^{1/3} \sim \frac{1}{T}\left(\frac{E}{\alpha_s M}\right)^{2/3}. \tag{4.29}$$

We note that the condition $\alpha_s\sqrt{ET^3} \ll M^2 \ll \alpha_s E^2$ defining the mass interval under consideration is equivalent to $\lambda \ll \tilde{L}^* \ll L^*$.

For $L \gg \tilde{L}^*$, the size of an effective scattering center responsible for the emission of one gluon is $\sim \tilde{L}^*$, and the dead cone suppression factor $\sim \mu_{\rm eff}/M$ stays frozen at the value

$$\left(\frac{\mu_{\rm eff}}{M}\right)_{\max} \sim \frac{\mu}{M}\sqrt{\frac{\tilde{L}^*}{\lambda}} \sim \left(\frac{\alpha_s\sqrt{ET^3}}{M^2}\right)^{2/3}. \tag{4.30}$$

In this region, the energy loss displays a linear dependence on L with the slope [48]

$$\Delta E(L \gg \tilde{L}^*) \sim \alpha_s E\,\frac{L}{\tilde{L}^*}\left(\frac{\mu_{\rm eff}}{M}\right)_{\max} \sim \alpha_s L\left(\frac{\mu^2 E}{\lambda M}\right)^{2/3} \sim \alpha_s^{7/3} T^2 L\left(\frac{E}{M}\right)^{2/3}. \tag{4.31}$$

The schematic plot of $\Delta E(L)$ looks like Fig. 4, but with two qualitative distinctions: (1) the scale L^* is replaced with $\tilde{L}^*$; (2) in the region between λ and $\tilde{L}^*$, $\Delta E(L) \propto \sqrt{L}$ [as in (4.26)] instead of $\Delta E(L) \propto \ln L$ in (3.33).

We now discuss the energy spectrum of emitted gluons. We consider the case $L \gg \tilde{L}^*$. We expect the spectrum to differ from that for light quarks [see (4.20) and Fig. 7] if the typical angle $\theta_{\rm typ}$ contributing to (4.20) becomes smaller than the parameter $\theta_M = M/E$. The typical angles associated with (4.20) are given by

$$\theta_{\rm typ}^2 \sim \frac{1}{\omega \ell_{\rm f}^{\rm med}(\omega)} \sim \sqrt{\frac{\mu^2/\lambda}{\omega^3}}, \tag{4.32}$$

where we use (4.15). The condition $\theta_{\rm typ} < \theta_M$ is hence equivalent to

$$\sqrt{\frac{\mu^2/\lambda}{\omega^3}} < \frac{M^2}{E^2} \Leftrightarrow \omega > \hat{\omega} \equiv \left(\frac{\mu^2 E^4}{\lambda M^4}\right)^{1/3} \sim T\left(\frac{\alpha_s E^2}{M^2}\right)^{2/3}.$$

We note that $L \gg \tilde{L}^*$ is equivalent to $\hat{\omega} \ll \omega_c$. When $\omega > \hat{\omega}$, the spectrum is given by

$$\omega\,\frac{{\rm d}I}{{\rm d}\omega} \sim \alpha_s \frac{L}{\ell_{\rm f}^{\rm med}}\frac{\theta_{\rm typ}^2}{\theta_M^2} \sim \alpha_s L\,\frac{\mu^2 E^2}{\lambda M^2}\,\frac{1}{\omega^2} \sim \alpha_s\sqrt{\frac{\omega_c \hat{\omega}^3}{\omega^4}} \quad (\omega > \hat{\omega}). \tag{4.33}$$

For $\omega < \hat{\omega}$, the spectrum is given by (4.20). The overall spectrum is shown in Fig. 9. We note that the behavior $\propto \omega^{-2}$ that we find for $\omega > \hat{\omega}$ differs from the behavior $\propto \omega^{-7/2}$ obtained in Ref. [26]. Integrating the spectrum, we recover the average loss in (4.31), which is dominated by $\omega \sim \hat{\omega}$. Noting that

$$\hat{\omega} \sim E\left(\frac{\mu_{\rm eff}}{M}\right)_{\max} \sim \frac{\mu E}{M}\sqrt{\frac{\tilde{L}^*}{\lambda}}, \tag{4.34}$$

we can rewrite average loss (4.31) in the compact form

$$\Delta E(L \gg \tilde{L}^*) \sim \alpha_s\,\hat{\omega}\,\frac{L}{\tilde{L}^*}, \tag{4.35}$$

which can be compared with the light-quark estimate in (4.16).

(C) $M^2 \gg a_s E^2$. Finally, for very large masses, the LPM effect does not play any role and BH linear law (4.24) holds for *all* lengths. Indeed, when M^2 exceeds $\alpha_s E^2$, the formation length $\tilde{L}^*$ becomes smaller than λ and gluons are emitted in individual incoherent scatterings. In this case, radiative losses are suppressed compared to collisional ones, as can be verified by comparing the slope in (4.24) with the slope $\sim \alpha_s^2 T^2$ for collisional loss. We therefore stress here that radiative loss (4.24) might be difficult or impossible to observe (even in a thought experiment). (See Section 6 for a further discussion of this point.)

As noted above, the spectrum of emitted gluons is soft in this case and is given by (4.23) times the number of scatterings L/λ. The spectrum starts to decrease as $\sim \omega^{-2}$ at the scale $\mu E/M$ rather than at $\hat{\omega}$, as it did in the intermediate mass region.

The linear energy dependence $\Delta E(L) \propto E$ may suggest the description of heavy-quark radiative losses in terms of the radiation length, as is usually done for ultrarelativistic electrons in usual matter. But it is not convenient here for two reasons: (1) in contrast to ultrarelativistic electrons, collisional losses here dominate over radiative ones; (2) the spectrum of emitted gluons is soft and the energy loss fluctuations are much smaller, for example, than for electrons forming atmospheric showers.

5. Radiative loss of a particle produced in a plasma

We now consider a charged particle produced inside a plasma. This situation is much more natural for QCD, where an energetic parton can be produced in a hard partonic subprocess inside the hot medium formed in heavy-ion collisions. However, we start by considering the less natural but simpler QED case of an electric charge produced in a QED plasma. We then study the QCD case.

5.1 Hot QED plasma

5.1.1 Electron. When an energetic charged particle is created in a hard process, it radiates bremsstrahlung photons. This radiation occurs even when the particle is created in the vacuum, and should be distinguished from the medium-induced radiative loss.

In this section, we consider the case of a fast and light charged particle produced in a hot QED plasma (for example, we can think of deep inelastic scattering in a QED plasma, or of direct lepton production in a QGP), and focus on its *medium-induced* radiative loss. This loss is associated with the Fourier components of the particle radiation field coat that had a chance to be formed within the distance L traveled by the newborn particle in the plasma, such that those components can be released as emitted photons during subsequent rescatterings. In other words, only the photons whose formation length (3.19) does not exceed L contribute to the induced radiative loss:

$$\ell_f(\omega,\theta) \sim \frac{1}{\omega\theta^2} \lesssim L\,. \tag{5.1}$$

In the case of the asymptotic particle studied in Sections 3 and 4, we found some contributions to the energy loss arising from $\ell_f \gg L$. In particular, in the BH regime $L \ll \lambda$, electron energy loss (3.11) arises from the photon formation lengths $\ell_f \gg E/\mu^2 \gg L$ [see (3.22)]. Due to prescription (5.1), this contribution should now be disregarded. We should only count those photons whose formation length does not exceed L, which results in an additional suppression in medium-induced radiative losses. Thus, when a light particle is created inside a plasma, there is no BH regime whatsoever.[21] We see shortly into what kind of behavior it is transformed.

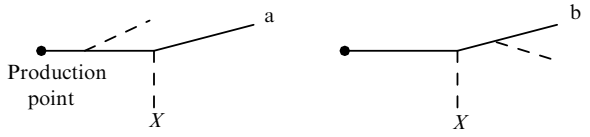

Figure 10. Photon radiation of an electron produced and scattered in a QED plasma.

On the other hand, the result in (3.26) [or, more accurately, (3.29)] for the radiative energy loss in a thick medium, $L \gg L^*$, should also hold when the particle is created not in the remote past but in the plasma. Indeed, result (3.26) corresponds to the formation lengths $\ell_f^{\rm med}(\omega) \sim \ell_f^{\rm med}(E) \sim L^* \ll L$, thus satisfying prescription (5.1). When $L \gg L^*$, the particle forgets the conditions of its birth.

We first consider the region $L \ll \lambda$. In this case, the particle undergoes one scattering with the probability $\sim L/\lambda$. The photon emission amplitude is given by the sum of the two diagrams in Fig. 10. For small photon frequencies $\omega \ll E$ and small scattering and emission angles, it can be evaluated as $\mathcal{M} \propto e\,\boldsymbol{\varepsilon}\,\mathbf{J}(L)$ with

$$\mathbf{J}(L) = \frac{\boldsymbol{\theta}'}{\theta'^2} - \frac{\boldsymbol{\theta}}{\theta^2}\left[1 - \exp\left(-\frac{i\omega L\theta^2}{2}\right)\right], \tag{5.2}$$

where L is the distance traveled by the particle between its production and scattering. We assume the particle to be massless. The term $\propto \boldsymbol{\theta}$ is the contribution of the diagram in Fig. 10a, and the term $\propto \boldsymbol{\theta}'$ is the contribution of the diagram in Fig. 10b.

Result (5.2) for the amplitude is rigorously derived in Appendix B, but its structure looks rather natural in the context of the above heuristic reasoning. When L is large compared to formation length (5.1), the rapidly oscillating factor $\sim \exp(-i\omega L\theta^2/2)$ can be dropped and the current $\mathbf{J}(L)$ is reduced to expression (3.5) for an asymptotic particle. On the other hand, for a photon formation length larger than L, the contribution of the diagram in Fig. 10a is suppressed and only the second diagram remains, corresponding to a photon emission from the final electron line, as in the absence of rescattering. Because we are interested in the medium-induced radiation intensity, we must subtract the last contribution from the scattering cross section, which yields

$$\omega\left.\frac{dI}{d\omega}\right|_{\rm induced} \sim \alpha\,\frac{L}{\lambda}\left\langle\int d^2\boldsymbol{\theta}\left(\left|\mathbf{J}(L)\right|^2 - \left|\mathbf{J}(0)\right|^2\right)\right\rangle$$
$$= 2\alpha\,\frac{L}{\lambda}\,{\rm Re}\left\langle\int d^2\boldsymbol{\theta}\,\frac{\boldsymbol{\theta}}{\theta^2}\left(\frac{\boldsymbol{\theta}}{\theta^2} - \frac{\boldsymbol{\theta}'}{\theta'^2}\right)\left[1 - \exp\left(-\frac{i\omega L\theta^2}{2}\right)\right]\right\rangle. \tag{5.3}$$

The averaging is done over the transverse momentum $\mathbf{q}_\perp$ exchanged in the scattering (we recall that $\boldsymbol{\theta}' \equiv \boldsymbol{\theta} - \boldsymbol{\theta}_s =$

[21] For heavy particles, this is not so (see the discussion below).

$\boldsymbol{\theta} - \mathbf{q}_\perp/E$). We average over the azimuthal directions of $\boldsymbol{\theta}_s$ first. Using the identity

$$\int \frac{d\phi}{2\pi}\left(\frac{\boldsymbol{\theta}}{\theta^2} - \frac{\boldsymbol{\theta}-\boldsymbol{\theta}_s}{(\boldsymbol{\theta}-\boldsymbol{\theta}_s)^2}\right) = \frac{\boldsymbol{\theta}}{\theta^2}\,\Theta(\theta_s^2-\theta^2)\,, \tag{5.4}$$

we obtain

$$\omega\,\frac{dI}{d\omega}\bigg|_{\text{induced}} \sim \alpha\,\frac{L}{\lambda}\left\langle \int \frac{d\theta^2}{\theta^2}\left(1-\cos\frac{\omega L\theta^2}{2}\right)\Theta(\theta_s^2-\theta^2)\right\rangle. \tag{5.5}$$

We must now average over θ_s^2 with the normalized probability $P(\theta_s^2)$ obtained by squaring the momentum Fourier harmonic of the screened Coulomb (Yukawa) potential [see (2.2)]:

$$P(\theta_s^2) = \frac{\mu^2/E^2}{(\theta_s^2+\mu^2/E^2)^2}\,. \tag{5.6}$$

The result is

$$\omega\,\frac{dI}{d\omega}\bigg|_{\text{induced}} \sim \alpha\,\frac{L\mu^2}{\lambda E^2}\int_0^\infty \frac{d\theta^2}{\theta^2(\theta^2+\mu^2/E^2)}\left(1-\cos\frac{\omega L\theta^2}{2}\right). \tag{5.7}$$

When $\omega L\mu^2/E^2 \ll 1$, which is true in the region $L \ll \lambda$ we are now considering, the integral is saturated by the emission angles[22]

$$\theta^2 \gtrsim \frac{1}{\omega L} > \frac{1}{EL} \gg \frac{1}{E\lambda} \gg \frac{\mu^2}{E^2}\,. \tag{5.8}$$

The integral in (5.7) is of the order of ωL. Hence, the spectrum is evaluated as

$$\omega\,\frac{dI}{d\omega}\bigg|_{\text{induced}} \sim \alpha\,\frac{L^2\mu^2}{\lambda}\,\frac{\omega}{E^2} \sim \alpha\,\frac{\omega\omega_c}{E^2}\,, \tag{5.9}$$

and the energy loss is given by

$$\Delta E(L \ll \lambda) \sim \alpha\,\omega_c \sim \alpha^3 T^3 L^2\,. \tag{5.10}$$

It is interesting to note the analogy with the discussion of the energy loss of an *asymptotic* and *massive* particle in Section 3.2. The effective cutoff $\theta^2 > 1/(EL)$ that arises here is similar to the 'dead cone' cutoff $\theta^2 > M^2/E^2$ in integral (3.38), with the parameter $\sqrt{E/L}$ playing the role of mass. Estimate (5.10) can actually be obtained by replacing $M^2 \to E/L$ in (3.43).

We see that $\Delta E(L)$ has not a linear but a quadratic dependence for small L. The reason for this is quite transparent, as we qualitatively explained before. When a hard electron is just born, its radiation field coat has not developed yet and the electron is not able to radiate. Roughly speaking, the *capacity* dE/dx to radiate vanishes at $L = 0$ and then increases linearly with L. The integration

$$\Delta E = \int_0^L dx\,\frac{dE}{dx} \tag{5.11}$$

yields another factor $\sim L$.

[22] The last inequality in (5.8) follows from $E \gg \lambda\mu^2 \sim T$. We also assume that $EL \gg 1$, i.e., even though L is smaller than λ, it is still larger than the wavelength of the energetic particle.

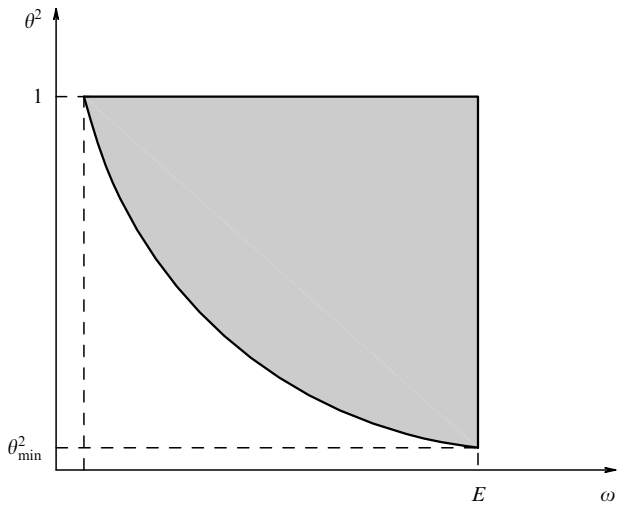

Figure 11. Photon energies and emission angles satisfying $\ell_f(\omega,\theta) < L$.

It is instructive to discuss a more heuristic derivation of estimate (5.10), not using the exact expression (5.2) of the radiation amplitude but simply consisting in integrating spectrum (3.6) (derived for an asymptotic particle) over ω and θ with the constraint $1/(\omega\theta^2) < L$. The corresponding integration domain is shown in Fig. 11. Because $\theta^2 \gg \mu^2/E^2$, the angular spectrum can be approximated by $\mu^2/(E^2\theta^4)$. The energy loss is then given by the expression

$$\Delta E(L \ll \lambda) \sim \alpha\,\frac{L}{\lambda}\int_0^E d\omega \int_{1/(\omega L)}^1 d\theta^2\,\frac{\mu^2}{E^2\theta^4} \sim \alpha\,\frac{L\mu^2}{\lambda E^2}\int_0^E d\omega\,\omega L \sim \alpha\,\omega_c \tag{5.12}$$

arising from typical values $\theta^2 \sim \theta^2_{\min} \sim 1/(EL)$ and $\omega \sim E$. This coincides with (5.10).

We emphasize, however, that although the simple and physically transparent argument given above leads to the correct result, it is heuristic and does not therefore allow detecting a subtle dynamical feature displayed in the accurate derivation based on (5.2).[23] Indeed, the argument leading to the heuristic estimate in (5.12) implicitly assumes that the momentum transfer is fixed at the value $q_\perp^2 = \mu^2$, i.e., it refers to a hypothetical model where Coulomb probability density (5.6) is replaced with $P(\theta_s^2) = \delta(\theta_s^2 - \mu^2/E^2)$ [corresponding to the scattering potential $V(r) \sim J_0(\mu r)$]. On the other hand, under the replacement $\theta_s^2 \to \mu^2/E^2$, expression (5.5), which follows from the diagram analysis, would yield

$$\omega\,\frac{dI}{d\omega}\bigg|_{q_\perp^2=\mu^2} \sim \alpha\,\frac{\omega^2 L^3\mu^4}{\lambda E^4}\,, \tag{5.13}$$

which leads to an energy loss that is suppressed compared to expression (5.12). Thus, estimate (5.12) fails for the hypothetical model where $P(\theta_s^2) = \delta(\theta_s^2 - \mu^2/E^2)$.

[23] In other words, the diagrams in Fig. 10 describing photon emission during a single scattering of a particle produced in a plasma dictate slightly different dynamics compared to the single-scattering diagrams for an asymptotic particle in Fig. 3 supplemented by constraint (5.1). On the other hand, the physical arguments that underlie the derivation of the multiple scattering dynamics based on single-scattering diagrams and the notion of the formation length seem to work in all cases.

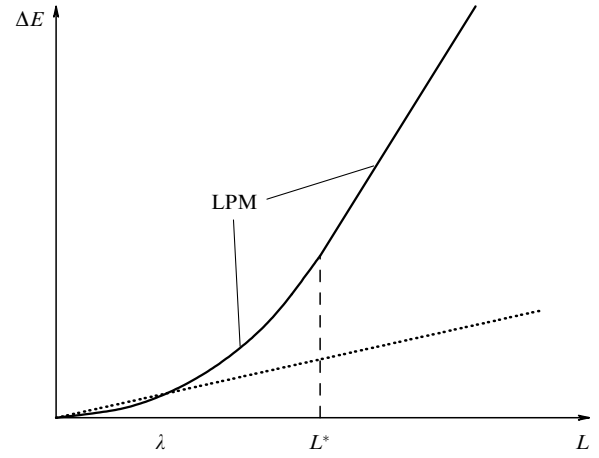

Figure 12. Radiative energy loss of an electron produced in a QED plasma. The quadratic dependence in (5.15) at $L \ll L^*$ is replaced by the linear dependence (3.29) at $L \gg L^*$. (Dotted line is the collisional loss.)

For the more realistic Yukawa potential, the results based on (5.5) and (5.12) are the same, but the integrals are saturated in different kinematical regions. With heuristic prescription (5.12), the characteristic radiation angle $\theta^2_{\rm rad} \sim 1/(\omega L)$ is much larger than the characteristic scattering angle $\theta^2_{\rm scat} \sim \mu^2/E^2$. In the more accurate formula (5.7), both angles are large [see (5.4)]:

$$\theta^2_{\rm rad} \sim \theta^2_{\rm scat} \sim \frac{1}{\omega L}\,. \tag{5.14}$$

A distinctive feature of the Yukawa scattering potential is that it allows very large transfers compared to the typical transfer $\sim \mu$. Thus, the constraints $\theta^2_{\rm s} \geqslant \theta^2$ [see (5.4)] and $\theta^2 \sim 1/(\omega L) \gg \mu^2/E^2$ [see (5.8)] can be realized simultaneously.

We now consider a larger medium, $L \gg \lambda$, with the Yukawa scattering potential. The electron is now scattered $N \sim L/\lambda$ times. If $L \ll L^*$, only one photon is emitted. The amplitude of photon emission in the multiple scattering process is evaluated accurately in Appendix B. It turns out that the leading contribution to the radiation spectrum arises from the region where *one* of the scattering angles is large, as in (5.14), while all other scattering angles are relatively small, $\sim \mu/E$. In other words, one of the N scattering momenta is $\sim \sqrt{E/L}$ (assuming $\omega \sim E$) and is much larger than the characteristic momentum transfer $\mu_{\rm eff} \sim \mu\sqrt{N}$ due to all other scatterings.[24] Any of the N scatterings can be distinguished in this way, which gives the factor $N \sim L/\lambda$ in the radiation spectrum. This is still given by integral (5.7), with the factor L/λ interpreted as the characteristic number of scatterings instead of the scattering probability. The estimate for the energy loss is still given by (5.10), which therefore holds in the extended range $L \ll L^*$,

$$\Delta E(L \ll L^*) \sim \alpha\,\omega_{\rm c} \sim \alpha^3 T^3 L^2\,. \tag{5.15}$$

Finally, for $L \gg L^*$, restriction (5.1) is not effective, as we already mentioned. We obtain the same dependence (3.29) as for a particle coming from infinity. The results are represented in Fig. 12. For large lengths, ΔE is linear in L, with $\mathrm{d}E/\mathrm{d}x \propto \sqrt{E}$, which is familiar from Sections 3 and 4. For L smaller than L^*, $\Delta E(L)$ displays quadratic dependence (5.15).

5.1.2 Muon. We now consider the radiative losses of a massive particle created in a plasma. As was also the case for a particle coming from infinity, the behavior of $\Delta E(L)$ is different in regions (3.41) and (3.47).

(A) $\boldsymbol{M^2 \ll \alpha\sqrt{ET^3}}$**.** We show that there is no difference with the case of light particles in this region, and the behavior of $\Delta E(L)$ is the same as in Fig. 12. We recall that for a massive particle, the vacuum formation length is given by (3.39).

When $L \ll L^*$, we showed previously that the induced radiative loss of a light QED particle arises from $\omega \sim E$ and $\theta^2 \sim 1/(\omega L) \sim 1/(EL)$. Therefore, if

$$\frac{1}{EL} \gg \theta^2_M = \frac{M^2}{E^2}\,, \tag{5.16}$$

then result (5.10) for a light particle also applies to a heavy particle. Intuitively, this happens when M is small compared to the effective 'mass' $\sim \sqrt{E/L}$ of the light particle [see the discussion below (5.10)]. To see that condition (5.16) is satisfied, we note that $M^2 \ll \alpha\sqrt{ET^3}$ implies $L^* \ll E/M^2$. When $L \ll L^*$, we have $M^2 \ll E/L^* \ll E/L$. Therefore, the result in (5.15) is also valid for a moderately massive particle.

The effects due to a nonzero mass are also irrelevant in the range $M^2 \ll \alpha\sqrt{ET^3}$ for large lengths $L \gg L^*$. Indeed, when $L \gg L^*$, the electron radiative loss arises from $\omega \sim E$ and the photon formation lengths $1/(\omega\theta^2)$ of the order of L^*, implying $\theta^2 \sim 1/(EL^*) \gg \theta^2_M$, where we again use $L^* \ll E/M^2$. Therefore, the result for a light particle in (3.29) is valid in the region $M^2 \ll \alpha\sqrt{ET^3}$.

An equivalent way to understand this is as follows. The length above which the mass can be neglected is determined by $\mu^2_{\rm eff} \sim (L/\lambda)\,\mu^2 \sim M^2$, i.e., by the scale L^{**} [see (4.27)]. For $M^2 \ll \alpha\sqrt{ET^3}$, we have $L^{**} \ll L^*$, and mass effects can *a fortiori* be neglected when $L \gg L^*$.

(B) $\boldsymbol{M^2 \gg \alpha\sqrt{ET^3}}$**.** In this region, the characteristic vacuum formation length $\ell_{\rm f} \sim E/M^2$ is smaller than the scale L^* and shows up first. Quadratic law (5.15) extends only up to the scale $L \sim E/M^2$, after which it is replaced by law (3.37), the same as for asymptotic and heavy QED particles.

5.2 Quark–gluon plasma

5.2.1 Light parton. An energetic, high-$p_\perp$ light parton produced in a proton–proton collision can be 'observed' via the jet of hadrons that it produces. These hadrons are the products of the parton bremsstrahlung induced by its sudden acceleration at the moment of its creation. In the process of building its asymptotic ($t \to +\infty$) field coat, the initially 'bare' parton radiates quasicollinear DGLAP gluons. The parton energy at the time of its production can in principle be determined by measuring the total jet energy.

If the parton is produced in a finite-size plasma, the parton energy loss due to its rescatterings in a hot medium can affect the structure of the hadron jet. In particular, this medium-induced energy loss leads to the suppression of large-$p_\perp$ hadrons (jet quenching) in ultrarelativisitic heavy-ion collisions compared to proton–proton collisions. Also, medium-induced gluon radiation enhances the hadron multiplicity within the jet. Here, we want to derive the medium-induced radiative energy loss of a light quark. As

[24] The condition $\sqrt{E/L} \gg \mu\sqrt{L/\lambda}$ is equivalent to $L \ll L^*$.

explained in Section 5.1, the formation length of the medium-induced gluon radiation must be smaller than L [see (5.1)].

We first consider the region $L \ll \lambda$. The physics is the same as in the Abelian case, with the only difference that the characteristic Abelian radiation cone width $\sim \mu/E$ must be replaced with the non-Abelian one $\sim \mu/\omega$ [see Section 4.1 and the comments below (4.11)]. Thus, QED expression (5.7) is transformed into

$$\omega \left.\frac{\mathrm{d}I}{\mathrm{d}\omega}\right|_{\text{induced}}^{\text{QCD}} \sim \alpha_s \frac{L\mu^2}{\lambda\omega^2} \int_0^\infty \frac{\mathrm{d}\theta^2}{\theta^2(\theta^2+\mu^2/\omega^2)} \left(1-\cos\frac{\omega L\theta^2}{2}\right). \tag{5.17}$$

Spectrum (5.17) has two different forms, depending on whether the gluon vacuum formation length $\ell_f(\omega) \sim \omega/\mu^2$ is smaller or larger than L:

$$\omega \left.\frac{\mathrm{d}I}{\mathrm{d}\omega}\right|_{\text{induced}}^{\text{QCD}} \sim \alpha_s \frac{L}{\lambda} \ln\frac{L\mu^2}{\omega}, \qquad \omega < L\mu^2, \tag{5.18}$$

$$\omega \left.\frac{\mathrm{d}I}{\mathrm{d}\omega}\right|_{\text{induced}}^{\text{QCD}} \sim \alpha_s \frac{\omega_c}{\omega}, \qquad L\mu^2 < \omega < E. \tag{5.19}$$

The contributions of these regions to the induced energy loss are

$$\Delta E_{\text{QCD},1}(L \ll \lambda) \sim \alpha_s \omega_c, \tag{5.20}$$

$$\Delta E_{\text{QCD},2}(L \ll \lambda) \sim \alpha_s \omega_c \ln\frac{E}{L\mu^2}. \tag{5.21}$$

The second contribution is logarithmically enhanced.

Expression (5.21) for the light parton radiative loss in the BH region was obtained in Ref. [19]. Its origin is the same as in QED. Namely, the energy loss arises from radiation angles larger than the *typical* scattering angle, $\theta^2 \sim 1/(\omega L) \gg \mu^2/E^2$ in QED, and $\theta^2 \sim 1/(\omega L) \gg \mu^2/\omega^2$ in QCD. Hence, as was also the case for QED expression (5.10), the QCD loss in (5.21) is specific to a Yukawa scattering potential.

In the region $\lambda \ll L \ll L^*$ and for small enough frequencies, the medium effects come into play and the formation length is given by (4.15). We can distinguish two (or, rather, two and a half) regions in the spectrum.

(1) If $\ell_f^{\text{med}}(\omega) \ll L$, implying $\omega \ll \omega_c$, the spectrum is the same as for the asymptotic particle in the LPM regime [see (4.20) and Fig. 7]:

$$\begin{aligned} &\omega \left.\frac{\mathrm{d}I}{\mathrm{d}\omega}\right|_{\text{induced}} \sim \alpha_s \frac{L}{\lambda}, \qquad \omega < \lambda\mu^2, \\ &\omega \left.\frac{\mathrm{d}I}{\mathrm{d}\omega}\right|_{\text{induced}} \sim \alpha_s \sqrt{\frac{\omega_c}{\omega}}, \qquad \lambda\mu^2 < \omega < \omega_c. \end{aligned} \tag{5.22}$$

The last expression arises from the typical emission angles given in (4.32):

$$\theta^2 \sim \frac{1}{\omega \ell_f^{\text{med}}(\omega)} \sim \sqrt{\frac{\mu^2/\lambda}{\omega^3}} \gg \frac{1}{\omega L}. \tag{5.23}$$

The contribution of the region $\omega < \lambda\mu^2$ to the energy loss is small. The region $\lambda\mu^2 < \omega < \omega_c$ yields

$$\Delta E_1(\lambda \ll L \ll L^*) \sim \alpha_s \omega_c. \tag{5.24}$$

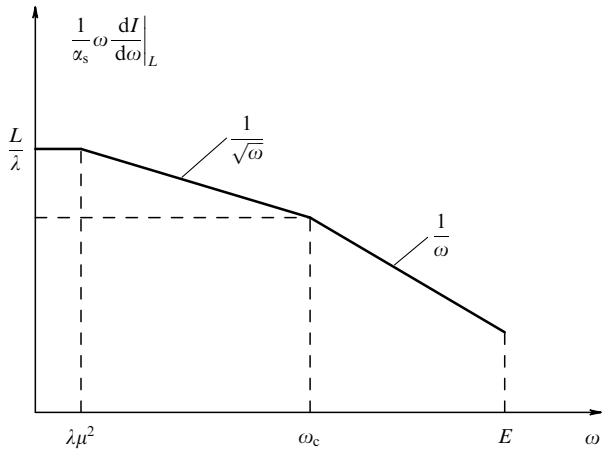

Figure 13. Induced gluon radiation spectrum of a light quark produced in a hot QCD medium for $\lambda \ll L \ll L^*$ (double logarithmic plot).

This contribution is specific to QCD [in QED, $\ell_f^{\text{med}}(\omega)$ exceeds L if it is smaller than L^*] and was identified in Refs [13, 17].[25]

(2) When $\omega > \omega_c$ (we note that $\omega_c \ll E$ if $L \ll L^*$), $\ell_f^{\text{med}}(\omega) > L$. In this case, the radiation spectrum is the same as for a single *effective* scattering with the typical scattering angle $N\mu^2/\omega^2$, where $N \sim L/\lambda$. The spectrum is then estimated from (5.17). Estimate (5.19) follows, but is now valid when $1/(\omega L) \gg N\mu^2/\omega^2$ (which exactly coincides with the condition $\omega \gg \omega_c$):

$$\omega \left.\frac{\mathrm{d}I}{\mathrm{d}\omega}\right|_{\text{induced}} \sim \alpha_s \frac{\omega_c}{\omega}, \qquad \omega_c < \omega < E. \tag{5.25}$$

This part of the spectrum arises from the typical angles

$$\theta^2 \sim \frac{1}{\omega L} \tag{5.26}$$

(meaning that the formation length is of the order of L), and contributes to the energy loss as

$$\Delta E_2(\lambda \ll L \ll L^*) \sim \alpha_s \omega_c \ln\frac{E}{\omega_c} \sim \alpha_s \omega_c \ln\frac{L^*}{L}. \tag{5.27}$$

This contribution was discussed in Ref. [19]. It is the QCD analog of QED expression (5.15) and depends on the presence of a long high-momentum tail in the Coulomb scattering potential.

The full radiation spectrum is represented in Fig. 13. In the region $\omega \ll \omega_c$, it is the same as for an asymptotic quark (see Fig. 7). In the region $\omega \gg \omega_c$, the spectrum is suppressed compared to the case of an asymptotic particle due to the constraint $\theta^2 \geqslant 1/(\omega L)$. This region still makes the dominant contribution to the energy loss, however.[26]

[25] We do not write the exact logarithmic factor $\propto \ln(L/\lambda)$ that may be involved in contribution (5.24) in general. As noted in [13, 17], such a logarithmic factor occurs in the case of the Coulomb scattering potential. It is not known, however, to what degree the statement about the presence of this factor is model independent.

[26] The hard part of the spectrum makes the leading contribution to the energy loss. Other quantities involving all the moments of the $\mathrm{d}I/\mathrm{d}\omega$ distribution, such as quenching factors [49], may also receive the leading contribution from the soft part of the radiation spectrum in (5.22).

For high energies, the contribution in (5.27) dominates that in (5.24).[27]

Finally, when $L \gg L^*$, the parameter ω_c becomes larger than E and ceases to play a role. The spectrum is given by (5.22) for all $\omega > \lambda\mu^2$, as for an asymptotic particle. Integrating over ω reproduces estimate (4.16) for the asymptotic particle energy loss in a thick medium.

The overall behavior of $\Delta E(L)$ is the same as in the Abelian case (see Fig. 12).[28] We stress again that the quadratic increase at small $L \ll L^*$ is a specific feature of the medium-induced energy loss of a newborn particle. It displays itself in both Abelian and non-Abelian plasmas.

5.2.2 Heavy quark. Finally, we discuss the radiative losses of a heavy quark created in a plasma. As was the case for an asymptotic quark, there are three main mass regions. But the case of a heavy quark produced in a plasma is more complicated. As we see in what follows, the second mass region $\alpha_s\sqrt{ET^3} \ll M^2 \ll \alpha_s E^2$ splits into two subdomains, where the logarithmic dependence of ΔE is slightly different.

(A) $\boldsymbol{M^2 \ll \alpha_s\sqrt{ET^3}}$**.** In this region, the dependence of $\Delta E(L)$ is the same as for light quarks. The reason for this is basically the same as in the Abelian case. The characteristic gluon radiation angle, which is of the same order as the photon radiation angle, as in (5.26), or exceeds it, as in (5.23), is much larger than θ_M^2 in the whole range of L and ω.

(B) $\boldsymbol{\alpha_s\sqrt{ET^3} \ll M^2 \ll \alpha_s E^2}$**.** In this range, the relevant in-medium formation length $\tilde{L}^*$ given in (4.29) is larger than λ, but smaller than the light-quark in-medium formation length L^*. The law $\Delta E(L) \sim L^2$ valid at small L is replaced by a linear dependence not at the scale L^* but at $\tilde{L}^*$. This is the main effect brought about by the quark mass.

In addition, there is a more subtle effect: the logarithmic factor multiplying $\alpha_s\omega_c$ in the estimate of $\Delta E(L)$ at small L might change. Indeed, the logarithmic factors in (5.21) and (5.27) come from integrating spectra (5.19) and (5.25) over the respective intervals $L\mu^2 < \omega < E$ and $\omega_c < \omega < E$. But a (large enough) mass leads to an effective cutoff in the spectrum when the characteristic angle $\sim 1/(\omega L)$ becomes smaller than θ_M^2. This happens when the gluon energy exceeds the scale

$$\omega_\square \equiv \frac{E^2}{LM^2}\,. \tag{5.28}$$

Beyond the scale $\omega_\square$, the spectrum rapidly decreases as $\sim 1/\omega^2$. This is a characteristic behavior of the hard part of energy spectra beyond the mass-induced cutoff [cf. (4.23) and Fig. 9]. Evidently, the statement above makes sense only when $\omega_\square < E$, i.e., when $L > E/M^2$. The results for $\Delta E(L)$ are slightly different, depending on whether $E/M^2 > \lambda$ (i.e., $M^2 < \alpha_s ET$) or $E/M^2 < \lambda$ (i.e., $M^2 > \alpha_s ET$). Representing the radiative loss as

$$\Delta E(L \ll \tilde{L}^*) \sim \alpha_s\,\omega_c \ln R\,, \tag{5.29}$$

we quote the estimates for R in the two relevant subregions.[29]

[27] This is true irrespective of whether the contribution in (5.24) involves a factor $\sim \ln(L/\lambda)$.

[28] As regards $\Delta E(L)$, the only difference between QED and QCD is the smooth logarithmic enhancement in (5.21) and (5.27).

[29] We do this for completeness, although the modification of the logarithm argument is probably too subtle an effect to be observed in experiment. In addition, some other logarithmic factors, unrelated to the integral $\int d\omega/\omega$, may occur (see footnote [25]).

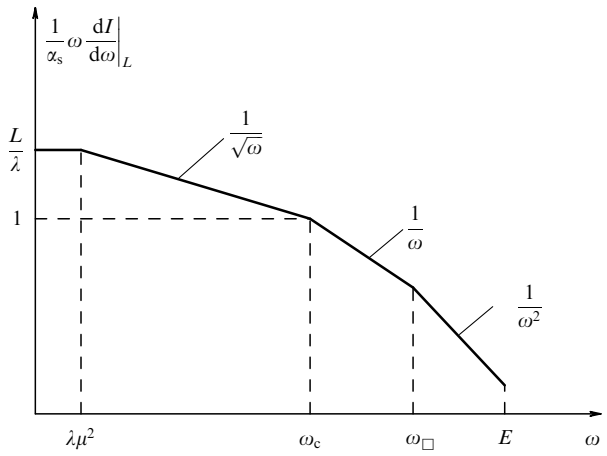

Figure 14. Induced gluon radiation spectrum of a heavy quark produced in a hot QGP for $\alpha_s\sqrt{ET^3} \ll M^2 \ll \alpha_s ET$ and $E/M^2 \ll L \ll \tilde{L}^*$ (double logarithmic plot).

(B1) $\boldsymbol{\alpha_s\sqrt{ET^3} \ll M^2 \ll \alpha_s ET}$**.** In this subregion, we have

$$R_{B1} = \begin{cases} \dfrac{E}{L\mu^2}\,, & L \ll \lambda\,, \\ \dfrac{E}{\omega_c}\,, & \lambda \ll L \ll \dfrac{E}{M^2}\,, \\ \dfrac{\omega_\square}{\omega_c}\,, & \dfrac{E}{M^2} \ll L \ll \tilde{L}^*\,. \end{cases} \tag{5.30}$$

In Fig. 14, for illustration, we show the induced radiation spectrum in the last case $E/M^2 \ll L \ll \tilde{L}^*$.

(B2) $\boldsymbol{\alpha_s ET \ll M^2 \ll \alpha_s E^2}$**.** Here, the estimates for R become

$$R_{B2} = \begin{cases} \dfrac{E}{L\mu^2}\,, & L \ll \dfrac{E}{M^2}\,, \\ \dfrac{\omega_\square}{L\mu^2}\,, & \dfrac{E}{M^2} \ll L \ll \lambda\,, \\ \dfrac{\omega_\square}{\omega_c}\,, & \lambda \ll L \ll \tilde{L}^*\,. \end{cases} \tag{5.31}$$

The logarithmic enhancement in $\Delta E(L)$ disappears at $L \sim \tilde{L}^*$, where the energy loss is

$$\Delta E(L \sim \tilde{L}^*) \sim \alpha_s\,\omega_c(\tilde{L}^*) \sim \alpha_s E\left(\frac{\alpha_s\sqrt{ET^3}}{M^2}\right)^{2/3}, \tag{5.32}$$

which is the same estimate as (4.30) and (4.31) for an asymptotic heavy quark. As was mentioned, when $L \gg \tilde{L}^*$, the quadratic law in (5.29) is replaced by a linear one, with the slope given in (4.31).

(C) $\boldsymbol{M^2 \gg \alpha_s E^2}$**.** When the mass is so large, the scale $\tilde{L}^*$ becomes smaller than λ. In this case, medium effects do not affect the formation length and it is given not by $E/(\mu_{\rm eff}M)$ [see (4.29)] but by $E/(\mu M)$ [see (4.25)]. At this scale, the quadratic law in L is replaced by linear law (4.24), the same as for an asymptotic heavy quark.

For $L \ll E/(\mu M)$, the energy loss is estimated as in (5.29). As in the previous case, the argument R of the logarithm depends on whether $L < E/M^2$ [in this case, the light-quark estimate in (5.21) still holds] or $L > E/M^2$ [in this case, the upper cutoff (5.28) is introduced in the spectrum]. To

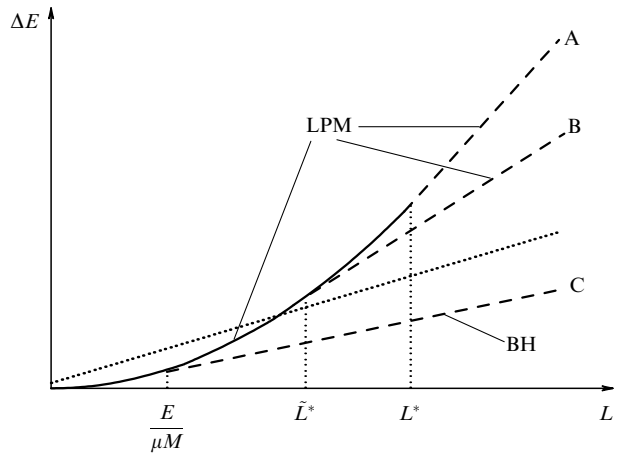

Figure 15. Induced radiative energy loss of a heavy quark produced in a QGP. A — $M^2 \ll \alpha_s\sqrt{ET^3}$, B — $\alpha_s\sqrt{ET^3} \ll M^2 \ll \alpha_s E^2$, C — $M^2 \gg \alpha_s E^2$. (Dotted line is the collisional loss.)

recapitulate,

$$R_C = \begin{cases} \dfrac{E}{L\mu^2}\,, & L \ll \dfrac{E}{M^2}\,, \\ \dfrac{\omega_\square}{L\mu^2}\,, & \dfrac{E}{M^2} \ll L \ll \dfrac{E}{\mu M}\,. \end{cases} \tag{5.33}$$

We observe that the law $\Delta E(L) \sim \alpha_s\,\omega_c \propto L^2$ is universal and is not modified at small enough L, no matter how large the quark mass is. On the other hand, the larger the mass, the earlier the change of regime between the quadratic law and the linear behavior. The slope of the line decreases as the mass increases. For $M^2 \gg \alpha_s E^2$, the slope is given by BH formula (4.24).

Our main results for a heavy quark produced in a plasma are qualitatively represented in Fig. 15. The transition between the quadratic and linear regimes occurs at a scale $\sim \min(L^*, \tilde{L}^*, E/(\mu M))$. It is L^* for $M^2 \ll \alpha_s\sqrt{ET^3}$, $\tilde{L}^*$ for $\alpha_s\sqrt{ET^3} \ll M^2 \ll \alpha_s E^2$, and $E/(\mu M)$ for $M^2 \gg \alpha_s E^2$.

6. Concluding remarks

The primary purpose of this review was, as for any other review, to bring together and systematically present known results scattered in original papers. Another goal was to rederive those results using simple physical arguments, rather than invoking complicated formalisms. For instance, we tried to explain the origin of the quadratic dependence $\Delta E_{rad} \sim L^2$ for thin plasmas or of the law $\Delta E_{rad} \sim L\sqrt{E}$ for thick plasmas in a semiheuristic way. But besides reviewing the known results, we have made some new observations.

First, we found that the L^2 law, which was generally believed to be a specific feature of QCD, is also valid in the Abelian case. The extra suppression at small L compared to a linear behavior $\Delta E_{rad}(L) \propto L$ is always present when a particle is created within the medium in a hard process. This is because a newborn particle needs time to develop its radiation field coat and acquire the capacity to radiate. We stress that although the Abelian and non-Abelian physical pictures and results are similar as regards the *average* radiative energy loss, the *spectra* of emitted photons in a QED plasma and of emitted gluons in a QGP are different [for thick plasmas, the corresponding spectra are given in (3.30) and (4.20)]. The difference is due to different kinematics of photon and gluon bremsstrahlung, as discussed in Sections 3 and 4. In QCD, the presence of the extra diagram in Fig. 6 (together with the diagrams in Fig. 3 with appropriate color factors) broadens the gluon angular spectrum [see (4.6) and (4.7)].

Another task we tried to accomplish was the systematic analysis of the radiative energy loss of a massive particle in the different regions of M and L. We have emphasized (see Fig. 15) that the mass effects play no role at small enough lengths, irrespective of how large the quark mass is. For $M^2 \ll \alpha_s\sqrt{ET^3}$, there is no effect at large L, either. For larger masses (where the main regions $\alpha_s\sqrt{ET^3} \ll M^2 \ll \alpha_s E^2$ and $M^2 \gg \alpha_s E^2$ should be distinguished), the heavy-quark loss $\Delta E_{rad}(L)$ starts to deviate from the light-quark loss at some critical length, which decreases as M increases.

We now discuss the question of the physical meaning of the mean free path λ. Definition (2.9) relates λ to the so-called *anomalous damping* ζ of ultrarelativistic collective excitations with quark or gluon quantum numbers [35]. The anomalous damping depends not on transport cross section (2.10) but on the total cross section ($\zeta \sim n\sigma^{tot}$). It is not the latter but the former that determines the scale of different transport phenomena, and a legitimate question is whether ζ (or equivalently λ) is a physical observable quantity.

This question was studied in Ref. [50]. No way to measure ζ was found there in the ultrarelativistic plasma, even in a thought experiment, but it was found that in a nonrelativistic (Boltzmann) plasma and in a certain range of parameters, ζ shows up in the argument of Coulomb logarithms describing transport phenomena.

Returning to the energy loss problem, we see that λ enters most formulas not alone but in the transport coefficient

$$\hat{q} = \frac{\mu^2}{\lambda} \sim \alpha_{(s)}^2 T^3\,. \tag{6.1}$$

For example, estimate (3.26) for the electron radiative loss in a thick plasma is represented as $\Delta E_{rad}(L \gg L^*) \sim \alpha L\sqrt{\hat{q}E}$. The parameter $\hat{q}$ describes how the transverse momentum of the particle increases with distance, $\langle q_\perp^2(L)\rangle = \hat{q}L$. To be more precise, $\hat{q}$ is given by [cf. (2.4)]

$$\hat{q} \sim n\int_{\mu^2}^{|t|_{max}} \frac{d\sigma}{dt}\,|t|\,d|t| \propto \alpha^2 T^3 \ln\frac{ET}{\mu^2} \tag{6.2}$$

and hence depends logarithmically on the energy of the incoming particle. Recently, the coefficient of the logarithm in (6.2) was evaluated analytically [51].

Seemingly, the parameter λ may show up as a scale that distinguishes a very thin plasma $L \ll \lambda$, where the particle undergoes at most one scattering, from the intermediate region $\lambda \ll L \ll L^*$, where the multiple scattering kinematics is effective. In our whole discussion, we indeed made a clear distinction between these two regions and treated them differently.

As regards the radiative energy loss of a particle created in a plasma, nothing essential happens at $L \sim \lambda$, as can be qualitatively seen in Fig. 12. But in the case of a light quark produced in a QGP and at $L \ll \lambda$, the parameter λ enters the argument of the logarithm in (5.21) (the relation $\mu^2 = \hat{q}\,\lambda$ must be used). But the domain $L \ll \lambda$ describes the rather marginal situation of a quark created near the plasma edge. Because tagging such quarks is unrealistic, whether λ can be

observed is questionable. In the more realistic case where $\lambda \ll L \ll L^*$, the logarithm in (5.27) depends only on the combination in (6.1). On the other hand, as we have already noted, the contribution from low frequencies $\omega \sim \omega_c$ may yield a logarithmic factor $\sim \ln(L/\lambda)$, leading to a weak logarithmic dependence on the scale $\sim \lambda$, which is observable in principle. This subtle question deserves further study.

For an asymptotic particle, the situation looks different. As is clear from Fig. 4, the dependence is essentially modified at $L \sim \lambda$. In addition, the slope of the curve in the BH region $L \ll \lambda$ is given by estimate (4.9), which explicitly involves λ. On the other hand, it is difficult to imagine how a plasma (in thermal equilibrium) of size $L \sim \lambda$ or less could be created, as we already mentioned in footnote [11].

Another attempt to pinpoint an explicit dependence on λ is associated with estimate (4.24) for the radiative energy loss of a heavy quark. We have seen that when the mass is sufficiently large, $M^2 \gg \alpha_s E^2$, this estimate is valid not only for unphysically thin plasmas, $L \ll \lambda$, but also for thick plasmas (see the dashed curve corresponding to $M^2 \gg \alpha_s E^2$ in Fig. 15). Expression (4.24) involves the combination $\mu/\lambda = \sqrt{\hat{q}/\lambda}$. But (4.24) describes only the *radiative* energy loss. And as we have seen, when $M^2 \gg \alpha_s E^2$, the radiative loss is suppressed compared to the *collisional* one. For light quarks, the radiative and collisional losses have different patterns: the characteristic energy of the radiated gluons is of the order of E, which is much larger than the characteristic energy transfer in one elastic collision. But the radiation spectrum of heavy quarks is soft. The spectrum is cut off beyond the scale $\mu E/M$, which for large masses $M^2 \gg \alpha_s E^2$ is smaller than the plasma temperature T. In other words, for such heavy quarks, it seems impossible to separate the radiative component of the net drag force $\mathrm{d}E/\mathrm{d}x$ and access μ/λ, and thus λ. Quite curiously, for smaller masses, when radiative losses dominate, their value is not sensitive to λ. For example, the nontrivial estimate in (4.31) depends only on $\hat{q}$ in the intermediate mass region $\alpha_s\sqrt{ET^3} \ll M^2 \ll \alpha_s E^2$.

Nevertheless, the parameter λ [and not only combination (6.1)] seems to have an independent physical meaning. In fact, this parameter appears under the logarithm in more refined estimates (3.29) and (4.19) for light-particle radiative losses (we recall that $T \sim \lambda\mu^2 = \hat{q}\lambda^2$). For the characteristic effective scattering momentum transfer, these estimates take the behavior $\sim (N \ln N)\,\mu^2$ (instead of $N\mu^2$) into account. In the developed LPM regime, $N = L^*/\lambda = \sqrt{E/(\lambda\mu^2)}$. Assuming that estimates (3.29) and (4.19) are correct,[30] the situation is then analogous to that observed in Ref. [50] for Boltzmann plasmas: the parameter λ affects observable quantities in a weak logarithmic way.

In other words, the physical status of λ (or ζ) in ultrarelativistic plasmas remains unclear. But it is indisputably very useful as a theoretical instrument that allows obtaining meaningful physical results for radiation spectra and energy losses.

[30] They were obtained in a model where the particle is scattered on a set of static Coulomb sources separated by the average distance λ. The presence of the factor $\propto \sqrt{\ln E}$ in (2.29) is a robust model-independent feature, the origin of the logarithm being the same as in (6.2). On the other hand, in what particular way the argument of the logarithm is formed, whether it is E/T, $ET/\mu^2 \sim E/(\alpha T)$, or some other ratio, is a more delicate and difficult question. Only an exact model-independent calculation (possibly using the formalism in Ref. [37]) can resolve it.

To top things off, we mention the fascinating issue of energy losses in $\mathcal{N} = 4$ supersymmetric Yang–Mills (SYM) theory. At weak coupling, there is not much difference with QCD, and we expect the estimates quoted in this paper to also apply to $\mathcal{N} = 4$ SYM. The main interest in the $\mathcal{N} = 4$ SYM theory is that in the large-N_c limit, many quantities can also be evaluated at a strong 't Hooft coupling $\lambda = g^2 N_c \gg 1$,[31] using the duality conjecture [52]. In particular, the drag force $\mathrm{d}E/\mathrm{d}x$ acting on a heavy quark moving through a thick $\mathcal{N} = 4$ SYM plasma is given by [53]

$$\frac{\mathrm{d}E}{\mathrm{d}x} = -\frac{\pi}{2}\sqrt{\lambda}\,T^2\,\frac{\sqrt{E^2 - M^2}}{M}\,, \qquad \lambda \gg 1\,. \tag{6.3}$$

This estimate is valid when $M \gg (\lambda T E^2)^{1/3}$ [48, 54]. Dependence (6.3) resembles the perturbative result in (4.24). One difference is that the latter is valid in a different mass region, namely $M \gg gE$, and that it describes only the radiative energy loss, which happens to be dominated by the collisional loss in this region.

In Refs [55] (see also [56]), the energy losses of light partons in a strongly coupled $\mathcal{N} = 4$ plasma were estimated. The dependence

$$\frac{\mathrm{d}E}{\mathrm{d}x} \sim -\lambda^{1/6}(E^2T^4)^{1/3} \tag{6.4}$$

for the *mean* drag force (for light partons, this quantity involves large fluctuations) was found. This is different from the perturbative dependence $\mathrm{d}E/\mathrm{d}x \propto \sqrt{E}$. More studies in this area are desirable.

Acknowledgments
We thank Yu Dokshitzer, F Arleo, P-B Gossiaux, and A Vainshtein for the useful discussions and comments. S.P. also thanks A Peshier for a fruitful collaboration on collisional energy loss, on which most of Section 2 in this paper is based.

7. Appendices

A. Typical momentum broadening in Coulomb rescattering
We here consider a charged (colored) particle with $E \to \infty$ moving in a perturbative QED (QCD) plasma and undergoing n successive Coulomb scatterings. The range $1/\mu$ of the Coulomb potential is assumed to be much shorter than the mean free path λ between two successive scatterings, and hence the elastic Coulomb rescatterings are considered independent. We calculate the typical transverse momentum $q_{\mathrm{typ}}(N)$ of the particle after N scatterings. In the case of a fixed coupling (QED), the result was found in Ref. [14] to be $q^2_{\mathrm{typ}}(N) \sim \mu^2 N \ln N$. We give an alternative derivation of this result and generalize it to a running coupling (QCD).

We first consider the Abelian fixed-coupling case. Coulomb scattering with the transverse momentum exchange $\mathbf{q}_i$ is associated with the normalized probability density

$$\frac{1}{\sigma_{\mathrm{tot}}}\frac{\mathrm{d}\sigma}{\mathrm{d}^2\mathbf{q}_i} \equiv P(\mathbf{q}_i) = \frac{1}{\pi}\frac{\mu^2}{(\mathbf{q}_i^2 + \mu^2)^2}\,, \qquad \int \mathrm{d}^2\mathbf{q}_i\,P(\mathbf{q}_i) = 1\,. \tag{A.1}$$

[31] Not to be confused with the mean free path!

The *average* momentum exchange $\langle \mathbf{q}^2 \rangle$ in a single Coulomb scattering is logarithmically divergent. (The divergence is cut off by the kinematical constraint on the maximal transverse exchange $|\mathbf{q}|_{\max}$, but we focus on the $E \to \infty$ limit, where $|\mathbf{q}|_{\max} \to \infty$.) On the other hand, the *typical* (median) transverse momentum transfer $q_{\rm typ}$, defined as the transfer such that the probability of having $|\mathbf{q}| < q_{\rm typ}$ is $1/2$, is well defined. Solving the equation

$$\int \mathrm{d}^2\mathbf{q}\, P(\mathbf{q})\, \Theta(q_{\rm typ}^2 - \mathbf{q}^2) = \frac{1}{2}\,, \tag{A.2}$$

we easily find that $q_{\rm typ}$ in one scattering equals the Debye mass μ.

We now determine the typical transfer $q_{\rm typ}(N)$ after N scatterings, defined by

$$\int \mathrm{d}^2\mathbf{q} \left(\prod_{i=1}^{N} \mathrm{d}^2\mathbf{q}_i\, P(\mathbf{q}_i) \right) \delta^2\!\left(\mathbf{q} - \sum_{i=1}^{N} \mathbf{q}_i \right) \Theta\big(q_{\rm typ}^2(N) - \mathbf{q}^2\big) = \frac{1}{2}\,. \tag{A.3}$$

Representing the δ-function as

$$\delta^2\!\left(\mathbf{q} - \sum_{i=1}^{N} \mathbf{q}_i \right) = \int \frac{\mathrm{d}^2\mathbf{r}}{(2\pi)^2} \exp\left[\mathrm{i}\mathbf{r}\left(\mathbf{q} - \sum_{i=1}^{N} \mathbf{q}_i \right) \right], \tag{A.4}$$

we use (A.3) to obtain

$$\frac{1}{2} = \int \frac{\mathrm{d}^2\mathbf{r}}{2\pi} \left[\tilde{P}(\mathbf{r}) \right]^N \int \frac{\mathrm{d}^2\mathbf{q}}{2\pi} \exp(\mathrm{i}\mathbf{r}\mathbf{q})\, \Theta\big(q_{\rm typ}^2(N) - \mathbf{q}^2\big)\,, \tag{A.5}$$

where

$$\tilde{P}(\mathbf{r}) = \int \mathrm{d}^2\mathbf{q}\, P(\mathbf{q}) \exp(-\mathrm{i}\mathbf{r}\mathbf{q}) = \mu r K_1(\mu r)\,. \tag{A.6}$$

The $\mathbf{q}$-integral in (A.5) can be done exactly, leading to

$$\begin{aligned} \frac{1}{2} &= \int_0^\infty \mathrm{d}r\, q_{\rm typ}(N)\, J_1\big(q_{\rm typ}(N)\, r\big) \left[r K_1(r) \right]^N \\ &= -\int_0^\infty \mathrm{d}r \left[r K_1(r) \right]^N \frac{\partial}{\partial r} J_0\big(q_{\rm typ}(N)\, r\big)\,. \end{aligned} \tag{A.7}$$

In the last equation and in what follows, r is expressed in units of μ^{-1}, and $q_{\rm typ}(N)$ in units of μ. Integrating by parts and using $(rK_1(r))' = -rK_0(r)$ we arrive at

$$\frac{1}{2} = N \int_0^\infty \mathrm{d}r\, r J_0\big(q_{\rm typ}(N)\, r\big) \big[r K_1(r) \big]^{N-1} K_0(r)\,. \tag{A.8}$$

Equation (A.8) for $q_{\rm typ}(N)$ was derived from (A.3) without any approximation. We now assume that the number of scatterings is large, $N \gg 1$, and derive the asymptotic behavior of $q_{\rm typ}(N)$ in this limit.

Clearly, when $N \gg 1$, the integral in (A.8) is saturated by $r \ll 1$. We can therefore approximate

$$K_0(r) \simeq -\ln r; \qquad r K_1(r) \simeq 1 - \frac{r^2}{4} \ln\frac{1}{r^2} \simeq \exp\left(-\frac{r^2}{4} \ln\frac{1}{r^2} \right). \tag{A.9}$$

Because $K_0(r)$ is a slowly varying function for $r \ll 1$, it follows from (A.8) that

$$\frac{1}{2} \simeq N \left\langle \ln\frac{1}{r} \right\rangle \int_0^1 \mathrm{d}r\, r J_0\big(q_{\rm typ}(N)\, r\big) \exp\left(-\frac{N r^2}{4} \ln\frac{1}{r^2} \right). \tag{A.10}$$

The integral is dominated by the region

$$N r^2 \ln\frac{1}{r^2} \sim 1 \underset{N \gg 1}{\Longleftrightarrow} r^2 \sim \frac{1}{N \ln N}\,. \tag{A.11}$$

Using this, we can rewrite (A.10) as

$$1 \simeq N \ln N \int_0^1 \mathrm{d}r\, r J_0\big(q_{\rm typ}(N)\, r\big) \exp\left[-(N \ln N)\, \frac{r^2}{4} \right]. \tag{A.12}$$

Setting $u = (N \ln N)\, r^2$, we rewrite (A.12) as

$$1 \simeq \int_0^\infty \frac{\mathrm{d}u}{2} J_0\left(\frac{q_{\rm typ}(N)}{\sqrt{N \ln N}} \sqrt{u} \right) \exp\left(-\frac{u}{4} \right). \tag{A.13}$$

Using

$$\int_0^\infty \mathrm{d}u\, J_0\big(C\sqrt{u}\big) \exp\left(-\frac{u}{4} \right) = 4 \exp\left(-C^2\right), \tag{A.14}$$

we finally obtain [reintroducing the dimension of $q_{\rm typ}(N)$]

$$q_{\rm typ}^2(N) \simeq (\ln 2)\, (N \ln N)\, \mu^2\,. \tag{A.15}$$

This result also immediately follows from the expression

$$f(q_\perp^2, N) \simeq \frac{1}{\pi \mu^2 N \ln N} \exp\left(-\frac{q_\perp^2}{\mu^2 N \ln N} \right) \tag{A.16}$$

for the probability distribution of the transverse momentum transfer $q_\perp^2$ after N scatterings, derived in Ref. [14]. Indeed, defining the typical transfer as in (A.3),

$$\int \mathrm{d}^2\mathbf{q}\, f(q^2, N)\, \Theta(q_{\rm typ}^2(N) - q^2) = \frac{1}{2}\,, \tag{A.17}$$

and using (A.16), we recover (A.15).

The derivation above was performed for a fixed coupling, and estimate (A.15) is therefore valid for QED. In QCD, the running of the coupling must be taken into account, and this brings about certain modifications. The effective coupling constant depends on the transverse momentum transfer q^2. The normalized probability density of a single Coulomb scattering is now

$$\begin{aligned} P(\mathbf{q})\Big|_{\rm QCD} &= \frac{1}{\pi} \frac{\mu^2}{(q^2+\mu^2)^2} \frac{\alpha_{\rm s}^2(q^2)}{\alpha_{\rm s}^2(\mu^2)} F\!\left(\frac{\mu}{\Lambda_{\rm QCD}} \right) \\ &\simeq \frac{1}{\pi} \frac{\mu^2}{(q^2+\mu^2)^2} \frac{\ln^2(\mu^2/\Lambda_{\rm QCD}^2)}{\ln^2(q^2/\Lambda_{\rm QCD}^2)}\,, \end{aligned} \tag{A.18}$$

where $F(x)$ is a smooth function that tends to unity in the limit $\mu \gg \Lambda_{\rm QCD}$ we are interested in, and which we can therefore choose as $F = 1$. The analysis is done along the same lines as in QED.

We first note that expression (A.8) can be rewritten for a general scattering probability density $\tilde{P}(\mathbf{r})$ as

$$\frac{1}{2} = -N \int_0^\infty \mathrm{d}r\, J_0\big(q_{\rm typ}(N)\, r\big) \big[\tilde{P}(\mathbf{r}) \big]^{N-1} \frac{\partial \tilde{P}(\mathbf{r})}{\partial r}\,. \tag{A.19}$$

If $N \gg 1$, we typically have $r \ll 1$ (with r expressed in units of μ^{-1}), implying that $\tilde{P}(\mathbf{r}) \simeq 1$ [see (A.21)]. Thus, (A.19) can be

approximated by

$$\frac{1}{2} \simeq N \int_0^\infty \mathrm{d}r\, J_0\big(q_{\mathrm{typ}}(N)\, r\big) \exp\big[-(N-1)\big(1-\tilde{P}(\mathbf{r})\big)\big] \times \frac{\partial}{\partial r}\big(1-\tilde{P}(\mathbf{r})\big)\,. \tag{A.20}$$

Using (2.18), we obtain (expressing q in units of μ)

$$\begin{aligned} 1-\tilde{P}(\mathbf{r}) &= \int \mathrm{d}^2\mathbf{q}\, P(\mathbf{q})\Big|_{\mathrm{QCD}} \big(1-\exp\left(-\mathrm{i}\mathbf{r}\mathbf{q}\right)\big) \\ &\simeq \int_0^{1/r^2} \mathrm{d}q^2\, \frac{1}{(q^2+1)^2}\, \frac{\ln^2\left(\mu^2/\Lambda_{\mathrm{QCD}}^2\right)}{\ln^2\left(q^2\mu^2/\Lambda_{\mathrm{QCD}}^2\right)}\, \frac{r^2q^2}{4} \\ &\simeq \frac{r^2}{4} \ln^2\left(\frac{\mu^2}{\Lambda_{\mathrm{QCD}}^2}\right) \int_1^{1/r^2} \frac{\mathrm{d}q^2}{q^2 \ln^2\left(q^2\mu^2/\Lambda_{\mathrm{QCD}}^2\right)} \\ &\simeq \frac{\alpha_{\mathrm{s}}(\mu^2/r^2)}{\alpha_{\mathrm{s}}(\mu^2)}\, \frac{r^2}{4} \ln\frac{1}{r^2}\,. \end{aligned} \tag{A.21}$$

Comparing with (A.9), we see that the running of α_{s} manifests itself in the factor $\alpha_{\mathrm{s}}(\mu^2/r^2)/\alpha_{\mathrm{s}}(\mu^2)$. Using (A.11), we now infer that the running of the coupling modifies the fixed-coupling estimate in (A.15) into the form

$$q_{\mathrm{typ}}^2(N)\Big|_{\mathrm{QCD}} \sim \frac{\alpha_{\mathrm{s}}(N\mu^2)}{\alpha_{\mathrm{s}}(\mu^2)}\, (N\ln N)\mu^2\,. \tag{A.22}$$

It is interesting to note that the typical momentum transfer at large N, in QED and QCD [see (A.15) and (A.22)], can be heuristically obtained from the formulas

$$q_{\mathrm{typ}}^2(N) \sim \mu^2 N \int_{\mu^2}^{q_{\mathrm{typ}}^2(N)} \frac{\mathrm{d}q^2}{q^2} \qquad (\mathrm{QED})\,, \tag{A.23}$$

$$q_{\mathrm{typ}}^2(N) \sim \mu^2 N \int_{\mu^2}^{q_{\mathrm{typ}}^2(N)} \frac{\mathrm{d}q^2}{q^2}\, \frac{\alpha_{\mathrm{s}}^2(q^2)}{\alpha_{\mathrm{s}}^2(\mu^2)} \qquad (\mathrm{QCD})\,. \tag{A.24}$$

We finally remark that (A.22) can also be represented as

$$q_{\mathrm{typ}}^2(N)\Big|_{\mathrm{QCD}} \sim \mu^2 N\, \frac{\ln\left(\mu^2/\Lambda_{\mathrm{QCD}}^2\right) \ln N}{\ln\left(\mu^2/\Lambda_{\mathrm{QCD}}^2\right) + \ln N}\,. \tag{A.25}$$

Hence, for *very* large N, namely $\ln N \gg \ln\left(\mu/\Lambda_{\mathrm{QCD}}\right)$, we obtain

$$q_{\mathrm{typ}}^2(N)\Big|_{\mathrm{QCD}} \sim N\mu^2 \ln\frac{\mu}{\Lambda_{\mathrm{QCD}}} \sim N\,T^2\,. \tag{A.26}$$

The scale T^2 is nothing but the average momentum transfer $\langle q_\perp^2\rangle$ associated with QCD probability density (A.18). In QED, this quantity is logarithmically divergent, but the running of α_{s} in QCD makes the integral for $\langle q_\perp^2\rangle$ convergent even when the upper bound is set to infinity, as can be seen from (A.24).

B. The LPM effect and Feynman diagrams

In the main body of this paper, we have operated mostly with heuristic arguments based on formation length estimates and single-scattering formulas. The same results can be derived by calculating the Feynman diagrams describing photon (gluon) radiation in the process of multiple scattering of a fast particle in a plasma. In this appendix, we do not attempt to perform a complete diagram analysis, but present some illustrative calculations that might help to better understand the origin of the LPM suppression. We restrict ourselves to the Abelian case and mostly follow the discussion in Ref. [41].

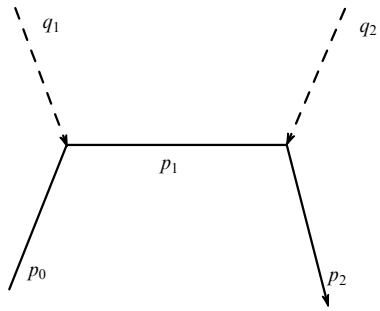

Figure 16. Electron elastic scattering on two centers.

As in Appendix A, we adopt the model where a scalar massless particle is scattered on static centers with a Yukawa potential:

$$V(\mathbf{x}) \sim \alpha \sum_i \frac{\exp\left\{-\mu|\mathbf{x}-\mathbf{x}_i|\right\}}{|\mathbf{x}-\mathbf{x}_i|}\,, \tag{B.1}$$

where $\mathbf{x}_i$ is the position of the ith center. We consider the case of only two such centers and assume that $\mathbf{x}_1 = \mathbf{0}$, $\mathbf{x}_2 = (\mathbf{x}_{2\perp}, z)$. Then the elastic scattering amplitude (Fig. 16) is given by

$$\mathcal{M}_{\mathrm{el}} \propto e^2 \int \frac{\mathrm{d}^3\mathbf{q}_1\, \mathrm{d}^3\mathbf{q}_2}{(\mathbf{q}_1^2+\mu^2)(\mathbf{q}_2^2+\mu^2)}\, \delta^{(3)}(\mathbf{q}_1+\mathbf{q}_2-\mathbf{q}) \times \exp\left(-\mathrm{i}\mathbf{q}_2\mathbf{x}_2\right) \frac{1}{p_1^2+\mathrm{i}\epsilon}\,. \tag{B.2}$$

The total momentum transfer $\mathbf{q}$ and the intermediate electron four-momentum p_1 are given by

$$\mathbf{q} = \mathbf{p}_2 - \mathbf{p}_0\,, \qquad p_1 = (E, \mathbf{q}_{1\perp}, E+q_{1\parallel})\,, \tag{B.3}$$

where we have chosen $p_0 = (E, \mathbf{0}_\perp, E)$. In the model of static centers, the energy transfer in each elastic scattering strictly vanishes, $q_1^0 = q_2^0 = 0$, which implies that $p_0^0 = p_1^0 = p_2^0 = E$.

We integrate over $\mathrm{d}q_{1\parallel}\, \mathrm{d}q_{2\parallel}\, \delta(q_{1\parallel}+q_{2\parallel}-q_\parallel)$ by closing the contour in the upper halfplane of $q_{1\parallel}$ and picking up the contribution of the pole in p_1^2 at the value[32]

$$p_{1\parallel} = E + q_{1\parallel} \simeq E - \frac{q_{1\perp}^2}{2E}\,. \tag{B.4}$$

Using the on-shell condition $p_2^2 = 0$, we obtain $q_\parallel \simeq -q_\perp^2/(2E)$, and from (B.2), we then obtain

$$\mathcal{M}_{\mathrm{el}} \propto e^2 \int \frac{\mathrm{d}^2\mathbf{q}_{1\perp}\, \mathrm{d}^2\mathbf{q}_{2\perp}}{(\mathbf{q}_{1\perp}^2+\mu^2)(\mathbf{q}_{2\perp}^2+\mu^2)}\, \delta^{(2)}(\mathbf{q}_{1\perp}+\mathbf{q}_{2\perp}-\mathbf{q}_\perp) \times \exp\left(-\mathrm{i}\mathbf{q}_{2\perp}\mathbf{x}_{2\perp}\right) \exp\left(\mathrm{i}\Phi_{\mathrm{scat}}\right), \tag{B.5}$$

[32] The contributions of the poles of $\mathbf{q}_1^2+\mu^2$ and $\mathbf{q}_2^2+\mu^2$ are suppressed by $\sim \exp\left(-\mu z\right) \ll 1$. Indeed, the distance between successive scattering centers is $z \sim \lambda$, where the mean free path λ satisfies $\lambda \sim 1/(e^2T) \gg \mu^{-1} \sim 1/(eT)$ in a perturbative plasma.

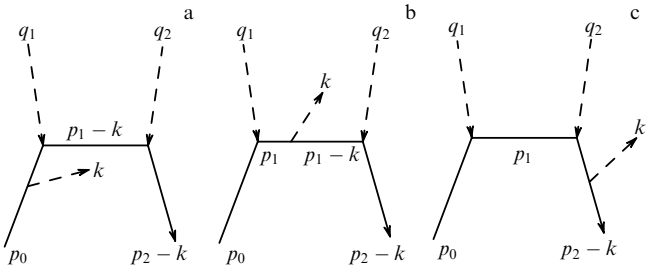

Figure 17. The amplitude of photon radiation induced by double elastic scattering.

where

$$\Phi_{\rm scat} = z(p_{1\parallel} - p_{2\parallel}) \approx \frac{z}{2E}\left[(\mathbf{q}_{1\perp} + \mathbf{q}_{2\perp})^2 - \mathbf{q}_{1\perp}^2\right]. \qquad \text{(B.6)}$$

To evaluate the elastic cross section, we fix the longitudinal distance z between the scattering centers and average $|\mathcal{M}_{\rm el}|^2$ over $\mathbf{x}_{2\perp}$. Integrating further over $\mathrm{d}^2\mathbf{q}_\perp$ yields

$$\sigma_{\rm scat} \propto \alpha^2 \int \frac{\mathrm{d}^2\mathbf{q}_{1\perp}\,\mathrm{d}^2\mathbf{q}_{2\perp}}{(q_{1\perp}^2 + \mu^2)^2 (q_{2\perp}^2 + \mu^2)^2}\,. \qquad \text{(B.7)}$$

We next consider the process where the scattered fast electron emits an additional photon. There are three graphs shown in Fig. 17.

It is convenient to define the momenta p_i as in the case of elastic scattering [see, e.g., (B.3)], such that the p_i 'do not know' about the emitted photon. On the other hand, the final momentum is now given not by p_2 but by $p_2 - k$, and the intermediate momentum $p_1 - k$ appears in the graphs in Fig. 17a and 17b. This shift of momenta leads to a modification of the phase factors in the amplitude. For different graphs, this modification is different, and now we cannot suppress the phase factors as we did in the case of elastic scattering, when passing from (B.2) to (B.7).

We now consider the details of the mechanism underlying the appearance of these phase factors. We first consider the graph in Fig. 17a. The conditions $(p_1 - k)^2 = 0$ and $(p_2 - k)^2 = 0$ respectively imply the relations

$$p_{1\parallel} \simeq E - \frac{p_{1\perp}^2}{2E} - \frac{\omega\theta_1^2}{2}\,, \qquad p_{2\parallel} \simeq E - \frac{p_{2\perp}^2}{2E} - \frac{\omega\theta_2^2}{2}\,, \qquad \text{(B.8)}$$

where $\theta_{1,2}$ are the angles between the direction of the emitted photon and $\mathbf{p}_1$ ($\mathbf{p}_2$). We assume that the angles are small.[33] Substituting expressions (B.8) in the phase $\Phi = z(p_{1\parallel} - p_{2\parallel})$, we obtain

$$\Phi_{\rm rad}^{\rm (a)} = \Phi_{\rm scat} + \frac{\omega z}{2}(\theta_2^2 - \theta_1^2) \qquad \text{(B.9)}$$

for the graph in Fig. 17a, with $\Phi_{\rm scat}$ given in (B.6). The corresponding contribution to the radiation amplitude is

$$\mathcal{M}_{\rm rad}^{\rm (a)} = -\frac{\boldsymbol{\theta}_0\,\boldsymbol{\varepsilon}}{\theta_0^2}\exp\left[\frac{\mathrm{i}\omega z}{2}(\theta_2^2 - \theta_1^2)\right]\mathcal{M}_{\rm el}\,, \qquad \text{(B.10)}$$

where $\boldsymbol{\theta}_0 = \mathbf{k}_\perp/\omega$ and $\boldsymbol{\varepsilon}$ is the photon polarization vector.

[33] Indeed, the radiation probability is dominated by small angles.

For the graph in Fig. 17c describing the emission from the final line, the structure $-\boldsymbol{\theta}_0\,\boldsymbol{\varepsilon}/\theta_0^2$ is transformed into $\boldsymbol{\theta}_2\,\boldsymbol{\varepsilon}/\theta_2^2$. The phase factor is different from that in the diagram in Fig. 17a due to different kinematics. In this case, putting the intermediate momentum on the mass shell gives not the condition $(p_1 - k)^2 = 0$ but $p_1^2 = 0$, and hence the expression for $p_{1\parallel}$ is not modified compared to the elastic scattering case. We have

$$\Phi_{\rm rad}^{\rm (c)} = \Phi_{\rm scat} + \frac{\omega z}{2}\,\theta_2^2\,, \qquad \text{(B.11)}$$

$$\mathcal{M}_{\rm rad}^{\rm (c)} = \frac{\boldsymbol{\theta}_2\,\boldsymbol{\varepsilon}}{\theta_2^2}\exp\left(\frac{\mathrm{i}\omega z}{2}\,\theta_2^2\right)\mathcal{M}_{\rm el}\,. \qquad \text{(B.12)}$$

The diagram in Fig. 17b provides two different contributions from the poles $p_1^2 = 0$ and $(p_1 - k)^2 = 0$. They both involve the structure $\boldsymbol{\theta}_1\,\boldsymbol{\varepsilon}/\theta_1^2$, but the residues have opposite signs. In addition, the phase factors for these two contributions are different. For the pole at $p_1^2 = 0$, the phase coincides with (B.11), whereas for the pole at $(p_1 - k)^2 = 0$, it coincides with (B.9). The sum of all contributions can be expressed as $\mathcal{M}_{\rm rad} = e\,\mathcal{M}_{\rm el}\,\boldsymbol{\varepsilon}\,\mathbf{J}$, where

$$\mathbf{J} = \mathbf{J}_1 \exp\left[\mathrm{i}\,\frac{\omega z}{2}(\theta_2^2 - \theta_1^2)\right] + \mathbf{J}_2 \exp\left(\mathrm{i}\,\frac{\omega z}{2}\,\theta_2^2\right), \qquad \text{(B.13)}$$

$$\mathbf{J}_1 = \frac{\boldsymbol{\theta}_1}{\theta_1^2} - \frac{\boldsymbol{\theta}_0}{\theta_0^2}\,, \qquad \mathbf{J}_2 = \frac{\boldsymbol{\theta}_2}{\theta_2^2} - \frac{\boldsymbol{\theta}_1}{\theta_1^2}\,. \qquad \text{(B.14)}$$

Each term in sum (B.13) corresponds to the radiation induced by elastic scattering on the associated center. The phase difference $\omega z\theta_1^2/2$ between the two terms can be interpreted as the phase acquired by a photon of energy ω in the frame moving with the fast particle [see (3.20)].

Result (B.13) can be easily generalized to the case of N scattering centers. We assume that their longitudinal positions are $z_n = (n-1)\lambda$, $n = 1, \ldots, N$. Then

$$\mathbf{J}(N) = \exp\left[\mathrm{i}\,\frac{\omega\lambda(N-1)}{2}\,\theta_N^2\right]\sum_{n=1}^{N}\mathbf{J}_n\exp(\mathrm{i}\Phi_n)\,, \qquad \text{(B.15)}$$

$$\mathbf{J}_n = \frac{\boldsymbol{\theta}_n}{\theta_n^2} - \frac{\boldsymbol{\theta}_{n-1}}{\theta_{n-1}^2}\,; \qquad \boldsymbol{\theta}_n \equiv \boldsymbol{\theta}_0 - \sum_{m=1}^{n}\frac{\mathbf{q}_{m\perp}}{E}\,, \qquad \text{(B.16)}$$

$$\Phi_n = -\frac{\omega\lambda}{2}\sum_{m=n}^{N-1}\theta_m^2\,, \quad n = 1, \ldots, N-1\,, \quad \Phi_N = 0\,. \qquad \text{(B.17)}$$

The radiation energy spectrum is

$$\omega\,\frac{\mathrm{d}I}{\mathrm{d}\omega} = \frac{\alpha}{\pi^2}\int \mathrm{d}^2\boldsymbol{\theta}_0\left|\sum_{n=1}^{N}\mathbf{J}_n\exp(\mathrm{i}\Phi_n)\right|^2. \qquad \text{(B.18)}$$

This should be averaged over $\mathbf{q}_{n\perp}$ with the weight

$$\prod_n \frac{\mu^2\,\mathrm{d}^2\mathbf{q}_{n\perp}}{\pi(q_{n\perp}^2 + \mu^2)^2}\,. \qquad \text{(B.19)}$$

The analysis of expression (B.18) confirms the physical picture outlined in Section 3. In particular, (i) the characteristic total scattering angle is $\theta_{\rm tot}^2 \sim N\mu^2/E^2$; (ii) the contributions of different scattering centers in (B.18) are coherent (and hence we are dealing in this case with one effective scattering) when $\omega N\lambda\theta_{\rm tot}^2 \sim \omega L\theta_{\rm tot}^2 \ll 1$, i.e., when $L \ll (\lambda E^2/(\omega\mu^2))^{1/2}$.

The scale $(\lambda E^2/(\omega\mu^2))^{1/2}$ coincides with $\ell_{\rm f}^{\rm med}(\omega)$ defined in (3.25). At $\omega \sim E$, the last quantity coincides with the characteristic in-medium formation length L^* (i.e., the coherence length whence one photon of energy $\sim E$ is emitted).

Results (B.15) and (B.18) were derived for an asymptotic particle. In the case where the particle is created in the medium, the radiation amplitude can be obtained from (B.15) by treating the position of the first scattering center as the creation point and by suppressing the contribution of the diagram analogous to Fig. 17a describing the emission from the initial line. Suppressing the irrelevant common phase factor in front of the sum in (B.15), changing $N \to N+1$ and the labeling $1 \to 0$, etc., we derive

$$\mathbf{J}_{\text{creation}+N\,\text{scatterings}} = \frac{\boldsymbol{\theta}_0}{\theta_0^2}\exp(\mathrm{i}\Phi_0) + \sum_{n=1}^{N}\mathbf{J}_n\exp(\mathrm{i}\Phi_n)\,. \quad \text{(B.20)}$$

For $N=1$, we reproduce the result in (5.2).

The medium-induced radiation spectrum is

$$\omega\,\frac{\mathrm{d}I}{\mathrm{d}\omega}\bigg|_N^{\text{induced}} \sim \int \mathrm{d}^2\boldsymbol{\theta}_0\left(|\mathbf{J}|^2 - \frac{1}{\theta_0^2}\right), \quad \text{(B.21)}$$

where the square of the first term in (B.20) (corresponding to the vacuum contribution) is subtracted, as in (5.3). We obtain

$$\omega\,\frac{\mathrm{d}I}{\mathrm{d}\omega}\bigg|_N^{\text{induced}} \sim \alpha\int \mathrm{d}^2\boldsymbol{\theta}_0\left[2\,\frac{\boldsymbol{\theta}_0}{\theta_0^2}\sum_{n=1}^{N}\mathbf{J}_n\cos(\Phi_0-\Phi_n) + \left|\sum_{n=1}^{N}\mathbf{J}_n\exp(\mathrm{i}\Phi_n)\right|^2\right], \quad \text{(B.22)}$$

which is conveniently represented as[34]

$$\omega\,\frac{\mathrm{d}I}{\mathrm{d}\omega}\bigg|_N^{\text{induced}} \sim \alpha\int \mathrm{d}^2\boldsymbol{\theta}_0\left\{2\,\frac{\boldsymbol{\theta}_0}{\theta_0^2}\sum_{n=1}^{N}\mathbf{J}_n\big[\cos(\Phi_0-\Phi_n)-1\big] + \sum_{n\neq m=1}^{N}\mathbf{J}_n\mathbf{J}_m\big[\cos(\Phi_n-\Phi_m)-1\big]\right\}. \quad \text{(B.23)}$$

It is obvious that the induced spectrum vanishes when $L=0$, because this implies that $\Phi_n = 0$ for all n.

We first consider the contribution of the first term in (B.23) and concentrate on a particular term in the sum $\sum_n$. As can be seen from (B.17), the phase difference $\Phi_n - \Phi_0$ is independent of $\boldsymbol{\theta}_n$, and hence of $\mathbf{q}_{n\perp}$. We can therefore average over $\mathbf{q}_{n\perp}$ before integrating. Averaging over azimuthal directions gives [see (5.4)]

$$\langle\mathbf{J}_n\rangle_{\text{azim}} = \left\langle\frac{\boldsymbol{\theta}_{n-1}-\mathbf{q}_{n\perp}/E}{(\boldsymbol{\theta}_{n-1}-\mathbf{q}_{n\perp}/E)^2} - \frac{\boldsymbol{\theta}_{n-1}}{\theta_{n-1}^2}\right\rangle_{\text{azim}} = -\frac{\boldsymbol{\theta}_{n-1}}{\theta_{n-1}^2}\,\Theta\left(\frac{q_{n\perp}^2}{E^2}-\theta_{n-1}^2\right). \quad \text{(B.24)}$$

Averaging further over $q_{n\perp}^2$ with weight (5.6), we obtain

$$\langle\mathbf{J}_n\rangle \sim -\frac{\mu^2}{E^2}\,\frac{\boldsymbol{\theta}_{n-1}}{\theta_{n-1}^2(\theta_{n-1}^2+\mu^2/E^2)}\,. \quad \text{(B.25)}$$

[34] We use that $\sum_n \mathbf{J}_n = \boldsymbol{\theta}_N/\theta_N^2 - \boldsymbol{\theta}_0/\theta_0^2$ and $\int \mathrm{d}^2\boldsymbol{\theta}_0\,(1/\theta_N^2 - 1/\theta_0^2) = 0$.

Thus, we obtain the contribution

$$\omega\,\frac{\mathrm{d}I}{\mathrm{d}\omega}\bigg|_{\text{1st term}}^{\text{induced}} \sim \alpha\,\frac{\mu^2}{E^2}\sum_{n=1}^{N}\int\frac{\mathrm{d}^2\boldsymbol{\theta}_0}{\theta_0^2}\,\frac{\boldsymbol{\theta}_0\boldsymbol{\theta}_{n-1}}{\theta_{n-1}^2(\theta_{n-1}^2+\mu^2/E^2)} \times\left[1-\cos\left(\frac{\omega\lambda}{2}\sum_{m=0}^{n-1}\theta_m^2\right)\right], \quad \text{(B.26)}$$

where, in each term of the sum, the averaging over $\mathbf{q}_{m\perp}$ with $m \neq n$ should still be performed.

We suppose that $L \ll L^*$ [otherwise the physics is the same as for the asymptotic particle, and there is no point in analyzing (B.23) instead of (B.18)]. Then $1/(\omega L) > 1/(EL) \gg N\mu^2/E^2$. Thus, bearing in mind that $\theta_0^2 \sim 1/(\omega L)$ (to be verified *a posteriori*) and $|\mathbf{q}_{(m\neq n)\perp}| \sim \mu$, we derive

$$m \neq n \Rightarrow \theta_m^2 \simeq \theta_0^2 \sim \frac{1}{\omega L} \gg N\,\frac{\mu^2}{E^2}\,. \quad \text{(B.27)}$$

We arrive at estimate (5.7) of the spectrum, giving [see (5.9)]

$$\omega\,\frac{\mathrm{d}I}{\mathrm{d}\omega}\bigg|_{\text{1st term}}^{\text{induced}} \sim \alpha\,\frac{\omega\,\omega_{\rm c}}{E^2}\,, \quad \text{(B.28)}$$

which contributes to the average loss as

$$\Delta E\big|_{\text{1st term}} \sim \alpha\,\omega_{\rm c}\,. \quad \text{(B.29)}$$

The integral is indeed dominated by angles of the order of $1/(\omega L)$.

We show now that for $L \ll L^*$, the contribution of the second term in (B.23) is suppressed compared to (B.28) and (B.29). The sum involves $\sim N^2$ terms. We consider one of these terms, for example, the term with $m=1$, $n=N$. The phase difference

$$\Phi_{1N} = \Phi_N - \Phi_1 = \frac{\omega\lambda}{2}\sum_{k=1}^{N-1}\theta_k^2$$

is independent of $\mathbf{q}_{n\perp}$ and we can average $\mathbf{J}_n$ over it as before. In addition, choosing $\boldsymbol{\theta}_1$ rather than $\boldsymbol{\theta}_0$ as the integration variable, we observe that Φ_{1N} is independent of $\mathbf{q}_{1\perp}$, and we can also average $\mathbf{J}_1$ over $\mathbf{q}_{1\perp}$. We obtain

$$\omega\,\frac{\mathrm{d}I}{\mathrm{d}\omega}\bigg|_{1N} \sim \alpha\,\frac{\mu^4}{E^4}\int\mathrm{d}^2\boldsymbol{\theta}_1\,\frac{\boldsymbol{\theta}_1\,\boldsymbol{\theta}_{N-1}(1-\cos\Phi_{1N})}{\theta_1^2(\theta_1^2+\mu^2/E^2)\theta_{N-1}^2(\theta_{N-1}^2+\mu^2/E^2)}\,. \quad \text{(B.30)}$$

In contrast to integral (B.26), this integral is not dominated by large angles with $\Phi_{1N} \sim 1$. Indeed, assuming $\theta_k \simeq \theta_1$, we are led to the integral

$$\sim\int_{N\mu^2/E^2}\frac{\mathrm{d}\theta^2}{\theta^6}\left[1-\cos(\omega L\theta^2)\right], \quad \text{(B.31)}$$

which is saturated by

$$N\,\frac{\mu^2}{E^2} \ll \theta^2 \ll \frac{1}{\omega L}\,, \quad \text{(B.32)}$$

and exhibits a logarithmic behavior. Expanding $\cos(\omega L\theta^2)$ [which we are allowed to do in view of (B.32)], multiplying the contribution of one term in the sum in the second term in

(B.23) by N^2, and neglecting the logarithmic factor that is irrelevant in the present discussion, we obtain the estimate

$$\omega \left.\frac{\mathrm{d}I}{\mathrm{d}\omega}\right|_{\text{2nd term}}^{\text{induced}} \sim \alpha \left(\frac{\omega\,\omega_{\mathrm{c}}}{E^2}\right)^2 . \tag{B.33}$$

Integrating this over ω gives the average loss

$$\Delta E\big|_{\text{2nd term}} \sim \alpha\,\frac{\omega_{\mathrm{c}}^2}{E} \sim \alpha E \left(\frac{L}{L^*}\right)^4 . \tag{B.34}$$

This is indeed suppressed by $\sim \omega_{\mathrm{c}}/E \sim (L/L^*)^2 \ll 1$ compared to contribution (B.29) of the first term in (B.23).

References

1. Jackson J D *Classical Electrodynamics* (New York: Wiley, 1999)
2. Lifshitz E M, Pitaevskii L P *Fizicheskaya Kinetika* (Physical Kinetics) (Moscow: Fizmatlit, 2007) [Translated into English (Oxford: Butterworth-Heinemann, 1995)]
3. Shuryak E D *Phys. Rep.* **61** 71 (1980)
4. Bjorken J D, Fermilab Preprint PUB-82/59-THY (1982)
5. Adcox K et al. (PHENIX Collab.) *Phys. Rev. Lett.* **88** 022301 (2002); nucl-ex/0109003; Adler S S et al. (PHENIX Collab.) *Phys. Rev. Lett.* **91** 072301 (2003); nucl-ex/0304022
6. Adler C et al. (STAR Collab.) *Phys. Rev. Lett.* **89** 202301 (2002); nucl-ex/0206011
7. Adler S S et al. (PHENIX Collab.) *Phys. Rev. Lett.* **96** 032301 (2006); nucl-ex/0510047
8. Abelev B I et al. (STAR Collab.) *Phys. Rev. Lett.* **98** 192301 (2007); nucl-ex/0607012
9. d'Enterria D, in *Relativistic Heavy-Ion Physics* (Landolt-Börnstein Series) (Berlin: Springer-Verlag, 2008) (to appear); arXiv:0902.2488
10. Airapetian A et al. (HERMES Collab.) *Eur. Phys. J. C* **20** 479 (2001); hep-ex/0012049; *Phys. Lett. B* **577** 37 (2003); hep-ex/0307023; *Nucl. Phys. B* **780** 1 (2007); arXiv:0704.3270
11. Albino S et al., arXiv:0804.2021
12. Baier R et al. *Phys. Lett. B* **345** 277 (1995); hep-ph/9411409
13. Baier R et al. *Nucl. Phys. B* **483** 291 (1997); hep-ph/9607355
14. Baier R et al. *Nucl. Phys. B* **484** 265 (1997); hep-ph/9608322
15. Baier R et al. *Nucl. Phys. B* **531** 403 (1998); hep-ph/9804212
16. Zakharov B G *Pis'ma Zh. Eksp. Teor. Fiz.* **63** 906 (1996) [*JETP Lett.* **63** 952 (1996)]; hep-ph/9607440
17. Zakharov B G *Pis'ma Zh. Eksp. Teor. Fiz.* **65** 585 (1997) [*JETP Lett.* **65** 615 (1997)]; hep-ph/9704255
18. Zakharov B G *Yad. Fiz.* **61** 924 (1998) [*Phys. Atom. Nucl.* **61** 838 (1998)]; hep-ph/9807540
19. Zakharov B G *Pis'ma Zh. Eksp. Teor. Fiz.* **73** 55 (2001) [*JETP Lett.* **73** 49 (2001)]; hep-ph/0012360
20. Gyulassy M, Lévai P, Vitev I *Nucl. Phys. B* **571** 197 (2000); hep-ph/9907461
21. Gyulassy M, Levai P, Vitev I *Phys. Rev. Lett.* **85** 5535 (2000); nucl-th/0005032
22. Gyulassy M, Levai P, Vitev I *Nucl. Phys. B* **594** 371 (2001); nucl-th/0006010
23. Landau L D, Pomeranchuk I *Dokl. Akad. Nauk SSSR* **92** 535, 735 (1953) [Translated into English, in Landau L *The Collected Papers of L.D. Landau* (New York: Pergamon Press, 1965) p. 589]
24. Migdal A B *Phys. Rev.* **103** 1811 (1956)
25. Feinberg E L *Usp. Fiz. Nauk* **132** 255 (1980) [*Sov. Phys. Usp.* **23** 629 (1980)], for a pedagogic review
26. Dokshitzer Yu L, Kharzeev D E *Phys. Lett. B* **519** 199 (2001); hep-ph/0106202
27. Baier R, Schiff D, Zakharov B G *Annu. Rev. Nucl. Part. Sci.* **50** 37 (2000); hep-ph/0002198
28. Thoma M H, Gyulassy M *Nucl. Phys. B* **351** 491 (1991)
29. Mrówczyński S *Phys. Lett. B* **269** 383 (1991)
30. Braaten E, Thoma M H *Phys. Rev. D* **44** 1298 (1991); **44** R2625 (1991)
31. Thoma M H *J. Phys. G* **26** 1507 (2000); hep-ph/0003016
32. Peshier A *Phys. Rev. Lett.* **97** 212301 (2006); hep-ph/0605294
33. Peigné S, Peshier A *Phys. Rev. D* **77** 014015 (2008); arXiv:0710.1266
34. Peigné S, Peshier A *Phys. Rev. D* **77** 114017 (2008); arXiv:0802.4364
35. Lebedev V V, Smilga A V *Ann. Physics* **202** 229 (1990); for a review, see Smilga A V *Phys. Rep.* **291** 1 (1997); hep-ph/9612347
36. Blaizot J-P, Iancu E *Phys. Rep.* **359** 355 (2002); hep-ph/0101103
37. Arnold P, Moore G D, Yaffe L C *JHEP* **0011** 001 (2000); hep-ph/0010177; *JHEP* **0305** 051 (2003); hep-ph/0302165
38. Ginzburg I F et al. *Pis'ma Zh. Eksp. Teor. Fiz.* **34** 514 (1981) [*JETP Lett.* **34** 491 (1981)]
39. Weinberg S *The Quantum Theory of Fields I* (Cambridge: Cambridge Univ. Press, 1995) Ch. 13; Smilga A V *Lectures on Quantum Chromodynamics* (River Edge, NJ: World Scientific, 2001) Lecture 10
40. See e.g. the review on ionization losses in Yao W-M et al. "Review of Particle Physics" *J. Phys. G* **33** 1 (2006)
41. Baier R et al. *Nucl. Phys. B* **478** 577 (1996); hep-ph/9604327
42. Anthony P L et al. (SLAC-E-146 Collab.) *Phys. Rev. D* **56** 1373 (1997); hep-ex/9703016; *Phys. Rev. Lett.* **75** 1949 (1995)
43. Hansen H D et al. *Phys. Rev. Lett.* **91** 014801 (2003)
44. Zakharov B G *Pis'ma Zh. Eksp. Teor. Fiz.* **64** 737 (1996) [*JETP Lett.* **64** 781 (1996)]; hep-ph/9612431; *Pis'ma Zh. Eksp. Teor. Fiz.* **78** 1279 (2003) [*JETP Lett.* **78** 759 (2003)]; hep-ph/0311063
45. Aitala E M et al. (Fermilab E791 Collab.) *Phys. Rev. Lett.* **86** 4773 (2001); hep-ex/0010044
46. Ashery D *Nucl. Phys. B Proc. Suppl.* **161** 8 (2006); hep-ex/0511052
47. Gunion J F, Bertsch G *Phys. Rev. D* **25** 746 (1982)
48. Marquet C, arXiv:0810.2572
49. Baier R et al. *JHEP* **0109** 033 (2001); hep-ph/0106347
50. Smilga A V *Can. J. Phys.* **71** 295 (1993)
51. Arnold P, Xiao W *Phys. Rev. D* **78** 125008 (2008); arXiv:0810.1026
52. Maldacena J M *Adv. Theor. Math. Phys.* **2** 231 (1998); hep-th/9711200; Gubser S S, Klebanov I R, Polyakov A M *Phys. Lett. B* **428** 105 (1998); hep-th/9802109
53. Herzog C P et al. *JHEP* **0607** 013 (2006); hep-th/0605158; Gubser S S *Phys. Rev. D* **74** 126005 (2006); hep-th/0605182
54. Fadafan K B et al., arXiv:0809.2869
55. Gubser S S et al. *JHEP* **0810** 052 (2008); arXiv:0803.1470; Hatta Y, Iancu E, Mueller A H *JHEP* **0805** 037 (2008); arXiv:0803.2481
56. Chesler P M et al., arXiv:0810.1985